12-2016

Optimal design of sound absorbing systems with microperforated panels

Nicholas Nakjoo Kim
Purdue University

Graduate School Form
30 Updated 12/26/2015

PURDUE UNIVERSITY
GRADUATE SCHOOL
Thesis/Dissertation Acceptance

This is to certify that the thesis/dissertation prepared

By Nicholas Kim

Entitled
OPTIMAL DESIGN OF SOUND ABSORBING SYSTEMS WITH MICROPERFORATED PANELS

For the degree of Doctor of Philosophy

Is approved by the final examining committee:

J. Stuart Bolton
Chair

George T. Chiu

Gregory A. Blaisdell

Jeffrey F. Rhoads

To the best of my knowledge and as understood by the student in the Thesis/Dissertation Agreement, Publication Delay, and Certification Disclaimer (Graduate School Form 32), this thesis/dissertation adheres to the provisions of Purdue University's "Policy of Integrity in Research" and the use of copyright material.

Approved by Major Professor(s): J. Stuart Bolton

Approved by: Jay P. Gore 11/18/2016
Head of the Departmental Graduate Program Date

OPTIMAL DESIGN OF SOUND ABSORBING SYSTEMS WITH MICROPERFORATED PANELS

A Dissertation

Submitted to the Faculty

of

Purdue University

by

Nicholas Nakjoo Kim

In Partial Fulfillment of the

Requirements for the Degree

of

Doctor of Philosophy

December 2016

Purdue University

West Lafayette, Indiana

To my father

ACKNOWLEDGEMENTS

Firstly, I appreciate to my advisor Professor J. Stuart Bolton for his support and perfect advice on my research and also on my life. He helped me through all the time of my study with great patience. I learned from how to overcome when I met an obstacle in research or in life. And also I am thankful to Professor Patricia Davies for guidance and consideration. I would also like to thank my committee members, Professor Blaisdell, Professor Chiu, and Professor Rhoads for their valuable guidance and support.

I am also grateful to the 3M Company for the financial support. Especially, I would like to thank to Jonathan H. Alexander, Thomas Herdtle, Ron W. Gerdes, and Tom Hanschen at 3M Company for their supports on my research.

I also would like to thank to my colleagues Hyunjun Shin, Yangfan Liu, Donghoon Kim, Seungkyu Lee, Janghyun Kim, Rui Cao, Tongyang Shi and Yutong Xue from Ray W. Herrick Laboratories.

I especially thanks to my beautiful girlfriend, Yeji Lim. She always supports and encourages me to endure the hardest time in my life with love and trust. I cannot finish my degree without her help.

And I wish to thank to my mother and brother for enduring the tough time without me. I dedicate my gratitude for their sacrifice to make me devote to research without any

worry. Eric Kim, my younger brother, he did his best to be able to go through tough time of my family even though I supposed to do,

And final note that I dedicate this dissertation to my father.

TABLE OF CONTENTS

Page

LIST OF TABLES

Table Page

LIST OF FIGURES

Figure Page

Figure Page

Figure Page

Figure Page

ABSTRACT

Kim, Nicholas Nakjoo. Ph.D., Purdue University, December 2016. Optimal Design of Sound Absorbing Systems with Microperforated Panels. Major Professor: J. Stuart Bolton, School of Mechanical Engineering.

As the development of technology makes economic prosperity and life more convenient, people now desire a higher quality of life. This quality of life is based not only on the convenience in their life but also on clean and eco-friendly environments. To meet that requirement, much research is being performed in many areas of eco-friendly technology, such as renewable energy, biodegradable content, and batteries for electronic vehicles.

This tendency is also obvious in the acoustics area, where there are continuing attempts to replace fiber-glass sound absorbers with fiber-free materials. The combination of microperfoated panels (MPP) (one of the fiber-free sound absorbing materials), usually in the form of a thin panel with small holes, and an air backing may be one of the preferred solutions. These panels can be designed in many ways, and usually feature many small (sub-millimeter) holes and typically surface porosities on the order of 1 percent. The detailed acoustical properties of MPPs depend on their hole shape, the hole diameter, the thickness of the panel, the overall porosity of the perforated film, the film's mass per unit area, and the depth of the backing air cavity. Together, these

parameters control the absorption peak location and the magnitude of the absorption coefficient (and the magnitude of the transmission loss in barrier applications). By an appropriate choice of these parameters good absorption performance can be achieved in a frequency range one or two octaves wide. That kind of solution may be adequate when it is necessary to control sound only in a specified frequency range (in the speech interference range, for example). However, in order to provide appropriate noise control solutions over a broader range of frequencies, it is necessary to design systems featuring multiple-layers of MPPs, thus creating what amounts to a multi-degree-of-freedom system and so expanding the range over which good absorption can be obtained.

In this research, three different situations were considered: one was studying the combination of microperforated panels with tapered holes and a specific depth of air backing space with a view to finding the trade-off between hole angle and surface porosity. Secondly, it was of interest to study the use of multiple-layer MPPs as functional absorbers. Finally, there is a study of the optimization of a multi-layer cylindrical duct liner that gives maximum axial attenuation. Note that "Functional Absorber" is the name given to a system that can be hung, in an industrial space, for example, to provide acoustic absorption. The duct applications of interest would be in HVAC systems, whether in buildings, automotive systems or personal ventilators. In both applications, the focus was on obtaining the best possible performance in the full speech interference range, which spans the range from 500 Hz to 4000 kHz. In each case, a transfer matrix method has been developed to calculate the transmission loss and absorption coefficients provided by the systems.

Note finally that the design of an N multiple-layer MPP system depends on $5N$-1 parameters, and so a general optimization becomes difficult in realistic cases when as many as ten layers might be used. Thus, the use of a genetic algorithm to optimize the system parameters has been adopted, since an algorithm of that sort can efficiently identify good solutions from a very large design space. The results, as presented in this thesis, show that it is possible to identify the best combination of MPP properties that improve the desired acoustic performance, whether absorption or transmission loss, in a prescribed frequency range.

CHAPTER 1. INTRODUCTION

1.1 Objective

As technology makes people's lives more convenient and improves the quality of their lives, people now desire clean and eco-friendly environments. This tendency is also shown in the acoustics area, where there is great interest in sound absorber design. To reduce noise, many sound absorber systems are currently in use, for example, fiberglass, foam, and so on. The microperforated panel, which is based on the Helmholtz resonator concept, is an increasingly popular sound absorbing material that can be used to reduce interior noise in a variety of architectural acoustic applications.

Since the perforated panel was first introduced in 1947 in an acoustical context, numerous studies about perforated panels and their application have been performed. The oscillatory movement of the air through the holes in the panel creates a mass element and also causes viscous dissipation, and the viscous dissipation, in turn, causes sound energy dissipation. The mass of the fluid in the small holes combines with the stiffness of the air in a backing space to create an equivalent single-degree-of-freedom resonator (i.e., a Helmholtz resonator). The tuning of this system, and hence the frequency range of peak absorption, can be adjusted by changing the hole parameters or the backing depth (i.e., the stiffness), or both.

In the case of the very small (i.e., micro) perforations considered here, usually much less than 1 mm in diameter, they are not easy to make by using manual drilling, for example, so that the cost of microperforated panels has typically been high. Recently, however, new manufacturing processes have allowed the manufacture of relatively low cost, polymeric microperforated materials. As a result, there is increasing interest in these panels. But to make the best use of microperforated panels, accurate prediction of their performance is needed.

To predict the performance of microperforated panels, the classical Maa theory, initially formulated for constant diameter cylindrical holes, is widely used. To improve the accuracy of those predictions, a number of *ad hoc* corrections have been suggested to account for different hole shapes or different frequency ranges, and many engineers have tried to change the associated end correction factors to fit with their experimental results. For example, recently, a new set of equations for the end correction factor, intended to decrease the discrepancy with measurement for all ranges of frequency, was formulated for a number of different hole geometries based on computational fluid dynamics calculations.

The acoustical properties of MPPs can be predicted from a knowledge of 6 parameters, which are the hole shape, the hole diameter, the thickness of panel, the overall porosity of the perforated film, the film's mass per unit area, and the depth of the backing air cavity. These parameters control the absorption peak location and the magnitude of the absorption coefficient (and the magnitude of the transmission loss in barrier applications). An appropriate set of these parameters can provide good absorption performance in a one or two octave band frequency range. That kind of solution may be

adequate when it is necessary to control sound only in a relatively narrow frequency range. However, in order to provide appropriate noise control solutions over a broader range of frequencies (over the entire speech interference range, for example), it is necessary to design system featuring multiple-layers of MPPs, thus creating what amounts to a multi-degree-of-freedom system and so expanding the range over which good absorption can be obtained.

In the present research, three different situations were considered: the first involves a single microperforated panel layer with tapered holes and a specific depth of air backing space in front of a hard wall. As noted before, a single MPP layer can create significant absorption only over one or two octave bands, so this part of the study was focused on finding the relation between hole shape and porosity in a way that can create good absorption at minimum cost. The second subject is a multiple-layer MPP that can be used as a functional absorber, and the third is as a multi-layer cylindrical duct liner.

Note that "Functional Absorber" is the name given to a system that can be hung, in an industrial space, for example, to provide acoustic absorption. The duct applications of interest would be in HVAC systems, whether in buildings, automotive systems or personal ventilators. In all applications, the focus was on obtaining the best possible performance in the full speech interference range, which spans the range from 500 Hz to 4000 kHz. In each case, a transfer matrix method has been developed to calculate the transmission loss and absorption coefficients provided by the systems.

Note finally that the design of an N multiple-layer MPP system depends on $5N$-1 parameters, and so a general optimization becomes difficult in realistic cases when as many as ten layers might be used. Thus, the use of a genetic algorithm to optimize the

system parameters has been adopted, since an algorithm of that sort can efficiently identify good solutions from a very large design space. The results, as presented in this thesis, show that it is possible to identify the best combination of MPP properties that improve the desired acoustic performance, whether absorption or transmission loss, or some combination of the two in a prescribed frequency range.

1.2 Organization

This thesis consists of ten chapters. In this chapter, the objective of the thesis work has been introduced. A literature review related to Helmholtz resonators, microperforated panels, and the genetic algorithm is presented in Chapter 2. In Chapter 3, the optimal design of a single microperforated panel with tapered holes and the relation between parameters is described; an equation defining the relation between parameters is also formulated. In Chapter 4, an optimization method to design multi-layer microperforated panel system is suggested. In Chapter 5 multiple layers of microperforated panels are considered as a functional absorber, with the intention of maximizing the dissipation of acoustic energy in the system, for normal and random incidence case. In Chapter 6, a barrier, intended to maximize transmission loss in the speech interference range, is considered for normal and random incidence, and is optimized by using the genetic algorithm. Next, in Chapter 7, the optimization of a multilayer barrier system intended for two simultaneously different purposes, i.e., dissipation and transmission loss, is considered. To reduce the calculation cost, the use of multi-layers, but all having the identical panel properties, is discussed next in Chapter 8, and the pros and cons of this simplified model are discussed. In Chapter 9, a

microperforated panel as a cylindrical duct liner is suggested and an optimal design for maximizing the transmission loss is described. The thesis concludes with Chapter 10 in which the main conclusions of the present work are summarized, and suggestions for future work are presented.

CHAPTER 2. LITERATURE REVIEW

2.1 Helmholtz Resonator

The Helmholtz resonator is one of the oldest sound absorber concepts and is based on a very simple idea. The Helmholtz resonator has been the subject of analytical research in the acoustics area for over 100 years. Many investigators, e.g., Helmholtz, Rayleigh, and Ingard, have contributed to the modeling of the basic principles of the Helmholtz resonator. The components of Helmholtz resonators can be classified into two parts: a cavity and a relatively small opening (which is the microperforated panel considered in the next section). The air trapped in the cavity creates a stiffness, the air accelerating through the small opening creates inertia, and viscous dissipation in the hole creates resistance. Thus the Helmholtz resonator is conceptually similar to a single-degree-of-freedom mechanical resonator. Classically, all elements of a Helmholtz resonator are small compared to a wavelength in the frequency range of interest. By changing the geometry of the Helmholtz resonator, the resonator can be tuned to absorb sound over a given frequency range. However the frequency range of good absorption is relatively small compared to that offered by porous materials if the resistance is not carefully optimized.

As noted, in the frequency range of good absorption, the Helmholtz resonator can be modeled as a simple mechanical system. The stiffness created by the air in the cavity

can be replaced by a spring, and the inertia of the air in the holes is equivalent to a mechanical mass. The resonance frequency at which absorption occurs is then determined by the value of the stiffness and the mass (Morse and Ingard, 1968), and can be expressed as

$$f_0 = \frac{1}{2\pi}\sqrt{\frac{k}{m}} = \frac{c_0}{2\pi}\sqrt{\frac{S}{Vl}} \tag{2.1}$$

where f_0 is the resonance frequency, k is the stiffness constant, m is the mass, c_0 is the sound speed in air, S is the cross-sectional area of the orifice, l is the orifice length, and V is the volume of the cavity. Since flow must converge into the aperture, an end correction is needed to account for the inertial effect of fluid exterior to the aperture accelerating into the hole. For a circular hole, Rayleigh (1894) suggested that the end correction should be $\delta_0 = \frac{8r}{3\pi}$, where r is the hole radius, so that the resonance frequency can be written as

$$f_0 = \frac{1}{2\pi}\sqrt{\frac{k}{m}} = \frac{c_0}{2\pi}\sqrt{\frac{S}{V(l+2\delta_0)}} \tag{2.2}$$

where both inner and outer end corrections are accounted for. An end correction for rectangular holes was subsequently suggested by Ingard (1953). Additional effects that occur when the wavelength is not large compared to the neck length were studied by Panton and Miller (1975).

The Helmholtz resonator causes energy dissipation by viscous shearing within the fluid exterior to the hole and in the viscous boundary layer in the neck itself. The energy dissipation at the surface may also have a thermal component, but the thermal resistance is typically very small relative to the viscous resistance (Stinson and Shaw, 1985), and so it is usually neglected: i.e., compressibility effects are generally not important in the neck of the resonator.

2.2 Microperforated Panel

The idea of combining perforated panels with air spaces to create absorbers was initially studied by Bolt (1947). He found that the acoustic impedance of the perforated facing could be expressed in terms of the number of holes per unit area, their diameter, and the thickness of the perforated sheet. In Bolt's work, one inch of porous material was used to occupy the air space between the perforated panel and a rigid backing; the porous material thus provided the energy dissipation in the system since the hole diameter was large and so the viscous dissipation the holes generated was relatively small. The absorption coefficients for the samples he considered approached 0.9. He found that the location of the peak could be shifted by changing the hole and backing space geometrical parameters when the surface porosity was fixed. He also found that fabric material placed over the holes could be used to provide a controllable hole resistance. Flexural resonances of the panel in which the holes were formed were neglected. Ingard and Bolt (1951) then published a paper with a more complete theory and more experimental data. To describe the effect of the porous material in the backing space, the flow resistivity was used.

Following these early papers, several different ways were suggested to calculate the impedance of perforated panels. Melling (1973) considered the behavior of the acoustic impedance for a range of perforation scales at medium and high incident sound pressure levels. Various theories were reviewed and explained in Melling's paper. He found, for example, that the resistive component of the perforate impedance showed relatively poor agreement with measurements compared with the reactance.

Maa (1975) then suggested an important new theory, which is still widely used today. Three related papers (1987, 1998 and 1999) were published subsequently. The Maa model can be separated into two parts, one being a linear component and the other being a non-linear component which becomes significant at high incident sound pressure levels. The linear component of the Maa model is derived from Rayleigh's formulation (1894) for wave propagation in narrow tubes. Based on those equations, Crandall (1926) modeled a perforated plate, and Maa further developed Crandall's model for the case of very small holes in which the oscillatory viscous boundary layer spans the hole. Maa observed that if the holes in the perforated sheet are small enough (i.e., below 1 mm in diameter), they can provide a high enough resistance to make the addition of other resistive elements unnecessary.

In Maa's papers the flow through the holes in the microperforated panel is assumed to be incompressible. The equation of motion, which was derived by a sequence of approximations from the Navier-Stokes equation, can be expressed as

$$\rho\dot{u} - \frac{\eta}{r_1}\frac{\partial}{\partial r_1}\left(r_1\frac{\partial}{\partial r_1}u\right) = \frac{\Delta p}{t} \tag{2.3}$$

where ρ is the air density, η is the dynamic viscosity of air, u is the axial particle velocity, $\dot{u}$ is the axial particle accelerations, ΔP is the pressure difference between the two ends of the hole, r_0 is the diameter of hole, and r_1 is the radial dimension. When it is supposed that the velocity is harmonic, the solution of Eq. (2.3) for the case of non-slip axial boundary conditions at the cylinder surface is

$$u(r_1) = -\frac{\Delta p}{\eta k^2 t}\left[1 - \frac{2}{kr_0}\frac{J_0(kr_1)}{J_0(kr_0)}\right] \tag{2.4}$$

where here the parameter $k = \sqrt{-j\omega\rho/\eta}$, and J_0 is the first kind of zero order Bessel function. After calculating the average axial velocity in the cylinder, the acoustic impedance of the small hole can be expressed in terms of the pressure and the average velocity as

$$Z_1 = \frac{\Delta p}{\bar{u}} = j\omega\rho t\left[1 - \frac{2}{x\sqrt{-j}}\frac{J_1(x\sqrt{-j})}{J_0(x\sqrt{-j})}\right]^{-1} \tag{2.5}$$

where x is now a parameter referred to by Maa as the perforation constant (defined as $x = d\sqrt{\omega\rho/4\eta}$), d is the hole diameter, ω is the angular frequency, t is the length of the hole, and J_1 is the first kind of first order Bessel function. A normalized specific normal acoustic transfer impedance for the perforated sheet can then be expressed as

$$z = \frac{j\omega t}{\sigma c}\left[1 - \frac{2}{x\sqrt{-j}}\frac{J_1(x\sqrt{-j})}{J_0(x\sqrt{-j})}\right]^{-1} \tag{2.6}$$

where c is the speed of sound, and σ is the surface porosity of the sheet.

Maa extended Eq. (2.6) by adding an end correction to account for the inertial effect of the converging and diverging flow into and out of the holes. Eq. (2.6) was also used by Guo et al. (2008). Maa adopted the resistive end correction suggested by Ingard (1953), to account for energy dissipation at the surface of the sheet as flow approaches the hole. Ingard called this effect a surface resistance, and the surface resistance on one side of the hole was defined as $R_s = \frac{1}{2}\sqrt{2\eta\rho\omega}$.

In the microperforated panel formulation of Guo et al., an end correction was added to the real part of the above expression as:

$$r = Re\left\{\frac{j\omega t}{\sigma c}\left[1 - \frac{2}{x\sqrt{-j}}\frac{J_1(x\sqrt{-j})}{J_0(x\sqrt{-j})}\right]^{-1}\right\} + \frac{\alpha 2R_s}{\sigma\rho c} \tag{2.7}$$

where r is here the real part of the specific normal acoustic impedance, R_s is the surface resistance, and α is a nominally frequency-independent factor introduced by Guo et al. to account for hole type. It was suggested by Guo et al., based on a comparison with measurements, that α should be set to 4 when the hole is sharp-edged, and should be set to 2 when the hole has a rounded edge. Maa also used the surface resistance for the end correction, but he did not include a factor to account for hole shape. To obtain a more accurate specific normal acoustic transfer impedance of the microperforated panel, Yoo and Bolton (2007) and Hou and Bolton (2009) also suggested their own end correction factors, based on comparisons with measured data.

In previous work by the author [Bolton and Kim (2010)], to obtain more accurate end correction factors, computational fluid dynamics calculations were used, and it was found that α needs to be made a function of frequency, and that α can be expressed as:

$$\alpha = (16.9\frac{t}{d} + 152.8)f^{-0.5}. \tag{2.8}$$

A number of researchers have also been interested in the impedance of microperforated panels with different hole shapes. Randeberg (2000) suggested a method to calculate the specific impedance of a perforated panel with horn-shaped holes. He calculated the impedance of the horn-shape hole by using an integration method based on the Maa theory. Sakagami et al. (2008) compared their experimental results, which were for a thick, tapered-hole, microperforated panel, with the solution given by Randeberg.

Herdtle et al. (2013) also created a new formula for tapered holes based on the results of CFD calculations. An integration method was used to obtain the impedance of a tapered hole without the end correction factor, and it can be expressed as:

$$Z_{taper} = \int_0^t \frac{j\rho\omega}{\sigma_x}\left[1 - \frac{2}{k_x\sqrt{-j}}\frac{J_1(k_x\sqrt{-j})}{J_0(k_x\sqrt{-j})}\right]^{-1} dx, \tag{2.9}$$

where Z_{taper} is the impedance without the end correction factor, the perforation constant $k_x = r_x\sqrt{\omega\rho/\eta}$, porosity $\sigma_x = \sigma r_x^2/r_1^2$, radius of the hole $r_x = r_1 + (r_2 - r_1)x/t$, r_1 is radius of inlet hole, and r_2 is radius of outlet hole. By comparison with the CFD results,

the impedance including the end correction factor was found to be a function of hole angle θ, and can be expressed as

$$Z_* = \frac{\frac{t}{3}\left(r_1^2 + r_1 r_2 + r_2^2\right) + \beta\left(\frac{\pi - 2\theta}{\pi} r_1^3 + \frac{\pi + 2\theta}{\pi} r_2^3\right)}{\frac{t}{3}\left(r_1^2 + r_1 r_2 + r_2^2\right)} Z_{taper}. \tag{2.10}$$

This result is currently considered to be the most accurate representation of the impedance of microperforated panels having tapered (and in the limit, cylindrical) holes.

2.3 Genetic Algorithm

In the present work, to identify the optimal configurations of microperforated treatments, the Genetic Algorithm (GA) has been used. The genetic algorithm was developed to solve optimization problems based on the mechanism of natural selection and genetics. The concept of the genetic algorithm was developed by Holland (1975) and its computational implementation was introduced by Goldberg (1989). The computational code of the standard genetic algorithm (SGA) consists of replication, crossover and mutation, and it works as illustrated in Figure 2.1.

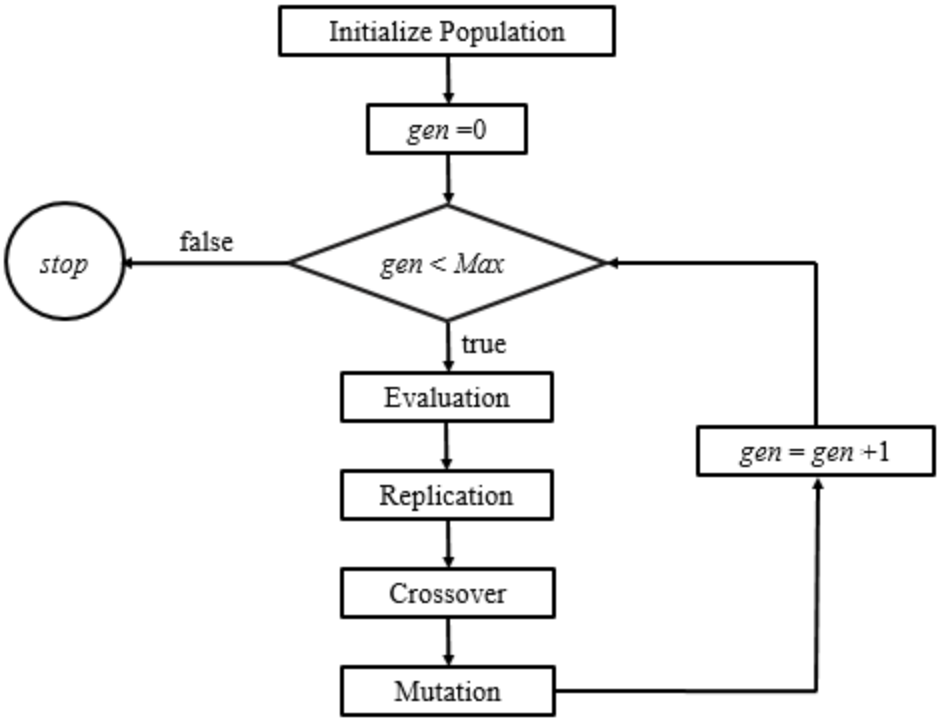

Figure 2.1. The flow chart of Standard Genetic Algorithm.

The procedure starts with a random population, and while a condition is true, the following steps will be executed: each individual of the population will be evaluated and an assignment of fitness will be performed, and then replication crossover and mutation is executed. Traditionally, the SGA procedure is repeated for a finite number of generations.

An initial population of individuals is needed, where the individuals in the population are the candidate solutions that are made to compete with each other for survival. Each individual is equivalent to the design parameters: here, the parameters of the microperforated panel design. When starting a GA, a genotypic domain is initially generated at random. An individual's genotype is a representation of its phenotype at a

lower level, analogous to the genetic sequences contained in the biological chromosomes. Then, they are decoded or mapped to phenotypes or the decision variables, which, in turn, will be evaluated and fitness assigned.

Replication or selection is the process of choosing the best individuals to participate in the production of offspring. This process is carried out stochastically and proportionally to the individual's fitness. Typical selection operators are "sampling with replacement" or "roulette wheel" selection (Goldberg 1989), "stochastic universal sampling", and "tournament selection". Unfortunately, Fonseca (1994) found that the roulette wheel selection (RWS) approach can result in large selection errors, and Deb (2001) suggested that it introduced a large variance in its realizations. An alternative selection approach is stochastic universal sampling (SUS), which is similar to the RWS process but with multiple, equally spaced pointers.

The next task is to create new solutions by mixing from the pool. The objective of recombination is to exchange genetic information with one another by bringing into a single individual the genetic features of two or more parents. Typically the reproduction is created by picking two solutions from the pool and performing a crossover operation between them. Each solution is split in two by the crossover point, which is chosen at random. Other typical recombination operators were also introduced by Booker (1987), Caruana et al. (1989), and Chipperfield et al. (1994).

In the mutation operator, individual genotypes are changed by some probabilistic rule. In other words there is a random change of some individuals. In artificial genetic algorithms, the mutation operator protects against an irrecoverable loss of some

potentially useful genetic material (Goldberg 1989). Fonseca (1994) calculated the probability of mutation p_m as:

$$p_m = 1 - \sigma^{-1/l} \tag{2.11}$$

where l is length of the chromosome, σ is the selective pressure, with a recommended value of 1.8.

Some applications have found difficulties with the binary representation of the population. Research in GA has brought continuous search space representation, so it can obtain any arbitrary precision in the optimal solution. Deb and Goyal (1996) applied polynomial mutation with the same replication operator.

In this work, to find the optimal point for multi-layer sound absorber system, the stochastic universal sampling method was used for the replication method and uniform crossover was used in crossover step.

CHAPTER 3. OPTIMAL DESIGN OF MICROPERFORATED PANELS WITH TAPERED HOLES

In this chapter, the design of single microperfoated panels is considered, and in particular panels with tapered holes. By an optimization process, it has been found that panels having wide range of taper angles give the same performance at different levels of surface porosity: i.e., there is a trade-off between porosity and hole taper. This result has important practical implication since it suggests that it is possible to obtain good result with relatively low porosity panels: i.e., panels having a relatively small number of holes per unit area, which would presumably be less expensive to manufacture than panels having a much larger number of holes per unit area.

3.1 Analytical Solution

To calculate the dynamic flow resistance for a microperforated panel with tapered holes analytically, an integration method, which was used by Randeberg (2000), can be used, based on the Guo model. The flow resistance of the Guo model can be divided into two parts, one part is from inner cylindrical section and the other part is from the outer region (i.e., the end corrections). To calculate the flow resistance of the first part, the tapered hole in the microperforated panel is divided into *N* short cylindrical holes with the thickness, $\Delta z = t/N$ (see Fig. 3.1). The specific impedance of the microperforated panel arising from the tapered hole sections can then he expressed by the sum:

$$Z_{taper} = \sum_{n=1}^{N} \frac{j\omega\Delta z}{\sigma_n c}\left[1 - \frac{2}{k_n\sqrt{-j}}\frac{J_1(k_n\sqrt{-j})}{J_0(k_n\sqrt{-j})}\right]^{-1} \quad (3.1)$$

where ω is the angular frequency, Δz is the thickness of the *n*th hole segment, *c* is the speed of sound, σ_n is the surface porosity of the *n*th sheet, k_n is the perforation constant defined by $k_n = d_n\sqrt{\omega\rho/4\eta}$, d_n is the diameter of *n*th hole segment, η is the dynamic viscosity, ρ is the air density, and J_0 and J_1 are the Bessel functions of the first kind of zero and first order, respectively.

Recently Herdtle et al. (2013) formulated a more accurate equation based on CFD calculation and integration method and it can be expressed as:

$$Z_* = \frac{\frac{t}{3}(r_1^2 + r_1 r_2 + r_2^2) + \beta\left(\frac{\pi - 2\theta}{\pi} r_1^3 + \frac{\pi + 2\theta}{\pi} r_2^3\right)}{\frac{t}{3}(r_1^2 + r_1 r_2 + r_2^2)} Z_{taper} \quad (3.2)$$

where Z_{taper} is the impedance without the end correction factor, the perforation constant $k_x = r_x\sqrt{\omega\rho/\eta}$, porosity $\sigma_x = \sigma r_x^2/r_1^2$, radius of the hole along its length $r_x = r_1 + (r_2 - r_1)x/t$, r_1 is radius of inlet hole, and r_2 is radius of outlet hole. Theoretically, the impedance of the panel with holes going from small large and from large to small, should be the same, so in Eq. (3.2), the inlet hole radius, r_1, was assumed to be smaller than the outlet hole diameter r_2. Note that lightweight, polymeric microperforated panels may be driven into motion by the sound pressure acting on the panel surface and by viscous drag generated by flow within the holes. Thus to account for the effect of the mass of the panel, the mass impedance, $j\omega m_s$ is added in parallel to the impedance of the rigid

microperforated panel with the tapered holes, where m_s is the mass per unit area of the panel. Finally, the total impedance of the panel is:

$$Z_{panel} = \frac{j\omega m_s Z_*}{j\omega m_s + Z_*} \tag{3.3}$$

In this chapter, the case of a single tapered hole microperforated panel with air backing terminated by a hard surface was considered, as shown as Figure 3.2. So, the impedance of total sound absorbing system can be expressed as

$$Z_{total} = Z_{panel} + Z_{air} = Z_{panel} - j\rho c \cot(kD) \tag{3.4}$$

where k is the wavenumber in the air space, which is ω/c, and D is the distance between the microperforated panel and hard surface, which is 0.02 m in this section. The normal incidence sound reflection coefficient and normal incidence sound absorption coefficient can be calculated as

$$R = \frac{Z_{total} - \rho c}{Z_{total} + \rho c} \tag{3.5}$$

$$\alpha = 1 - |R|^2, \tag{3.6}$$

where R is the reflection coefficient, and α is the absorption coefficient.

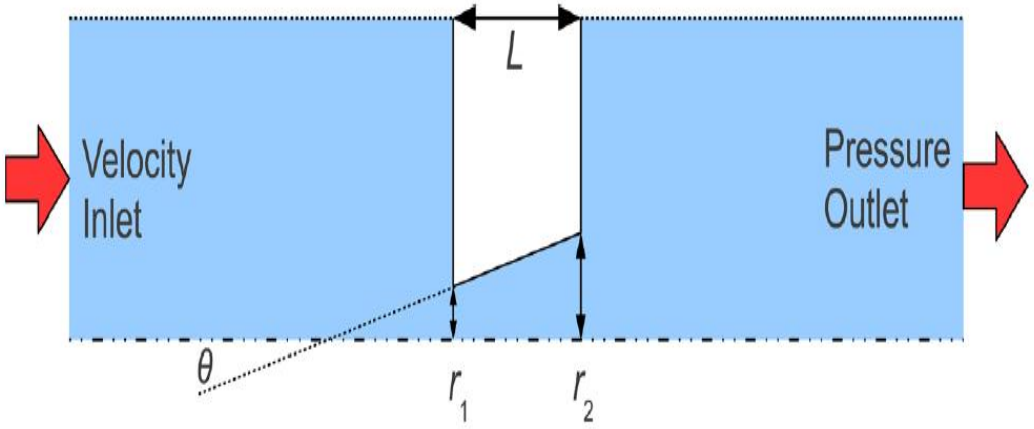

Figure 3.1. The geometry of a microperforated panel with tapered hole.

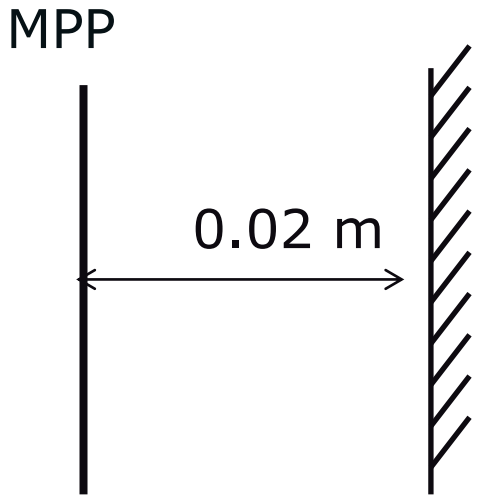

Figure 3.2. The geometry of a sound absorbing system.

3.2 Relation between Parameters

Here, only the normal incidence case was considered, and the flexural motion of the panel was ignored: that is, the panel can move only back and forth normal to its surface. To illustrate the trend of the acoustic properties of a single microperforated panel and to find the relationships between the parameters of a microperforated panel, one parameter was systematically varied at a time from the set of standard parameters. The standard parameters for the tapered hole microperforated panel were: the radius of inlet hole, 0.0001 m, the thickness of the panel, 0.0004 m, the porosity, σ_n, 0.02, the angle of the hole, 15°, and the mass per unit area, 1 kg/m^2. The air backing space was fixed to 0.02 m as shown as Figure 3.2. Figures 3.3 to 3.7 show the trends of the absorption coefficient caused by changing each parameter in turn: hole diameter, thickness of the panel, porosity, angle of hole, and mass per unit area. Note that the end of sound absorbing system is a hard wall, so the 1st and 3rd harmonics are visible in Figures 3.4 to 3.7. As shown in Figure 3.4, if the thickness of panel is made larger, the peak location of the absorption coefficient shifts to lower frequency, but there is no large impact in the overall frequency range. And as shown in Figure 3.7, if the panel is very light, the absorption coefficient goes to 0, since, in that cases the panel moves together with the sound field, and as a result there is no viscous dissipation in the hole. But if the panel is heavy enough, i.e., once the mass per unit area passes a certain threshold, there is no big impact on the absorption coefficient of the system by making the panel heavier. Further, the radius of the inlet hole, the porosity, and angle of the hole affect the absorption coefficient. As the radius of the holes is made smaller, the absorption coefficient of the system generally increases, as shown in Figure 3.3. And as shown as

Figure 3.6, if the angle of the hole is made larger, the absorption coefficient decreases. In Figure 3.5, it can be seen that peak locations and magnitude of absorption coefficient change significantly with changing porosity. So the radius of the inlet hole, porosity, and angle of the hole all affect the absorption coefficient, and, in particular, it was found that there was an inter-relationship between the taper angle of the hole and the surface porosity.

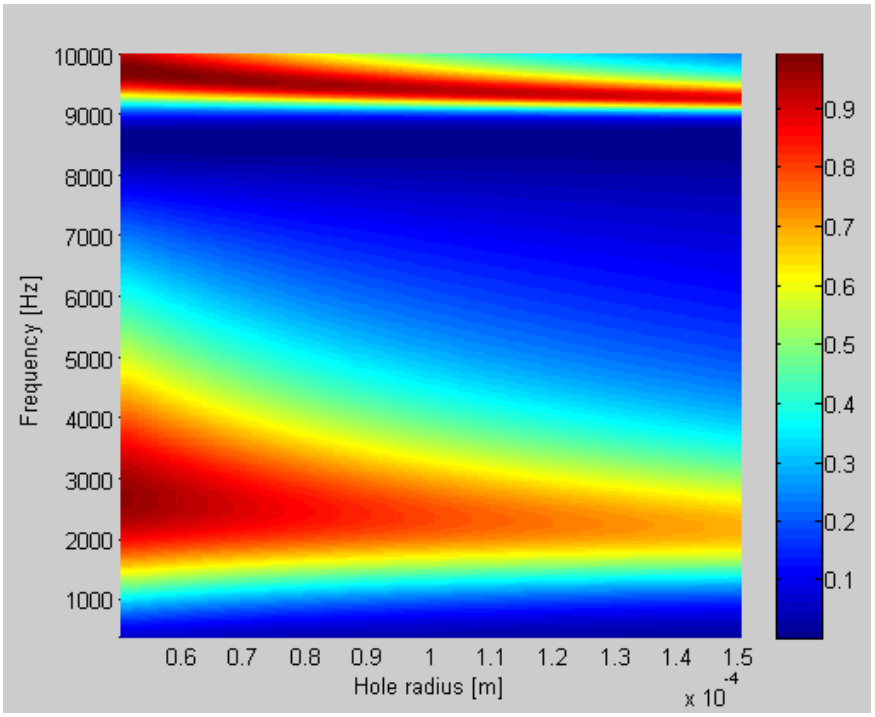

Figure 3.3. Absorption coefficient change due to hole radius.

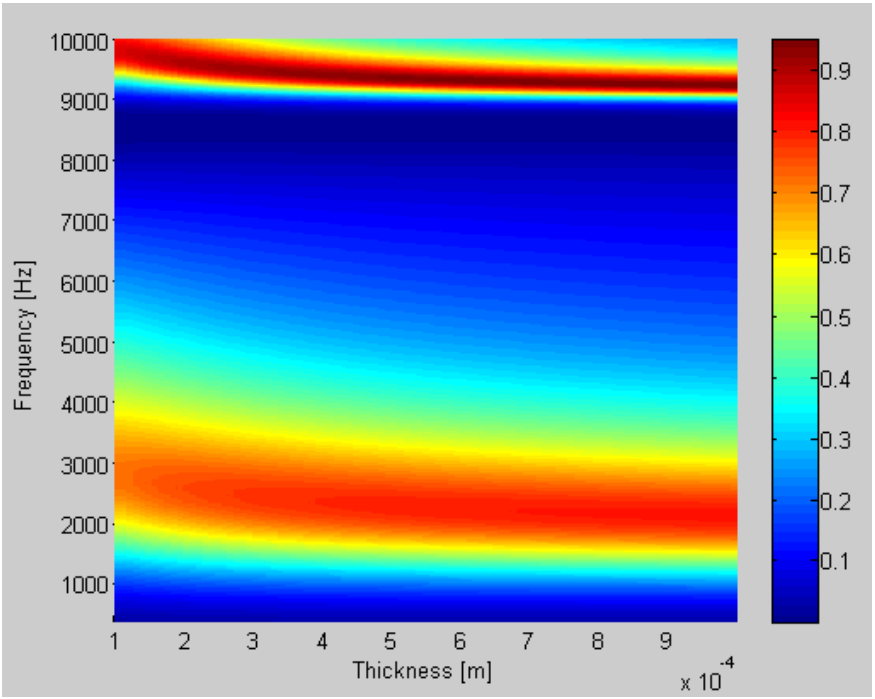

Figure 3.4. Absorption coefficient change due to thickness of panel.

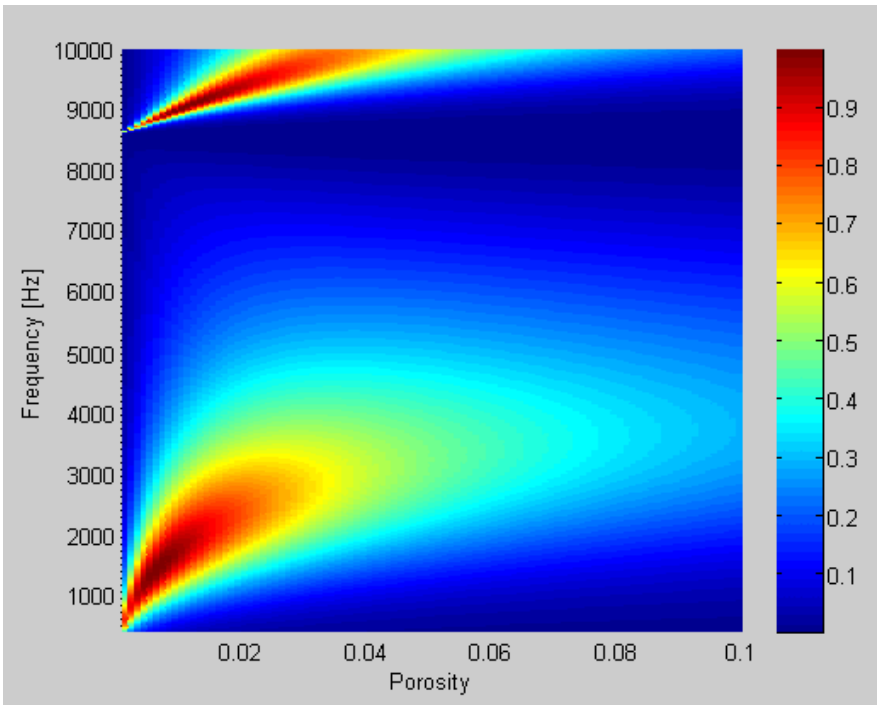

Figure 3.5.Absorption coefficient change due to porosity.

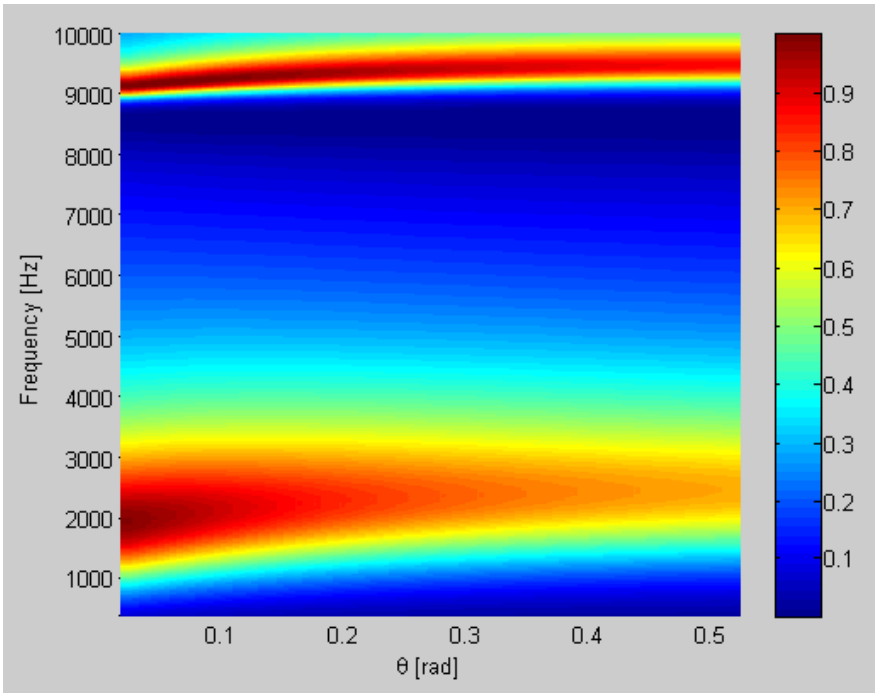

Figure 3.6. Absorption coefficient change due to hole angle.

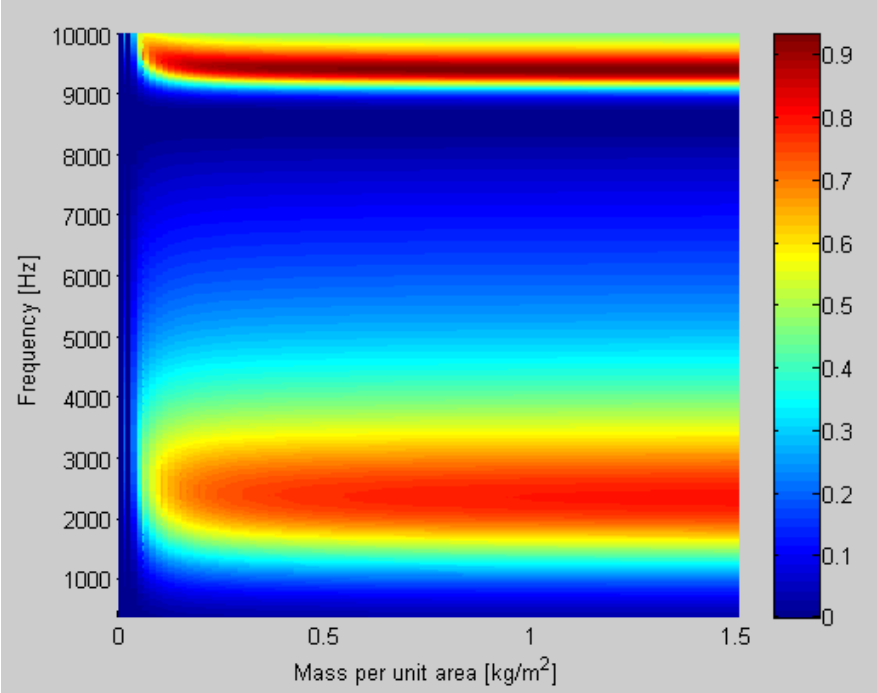

Figure 3.7. Absorption coefficient change due to mass per unit area.

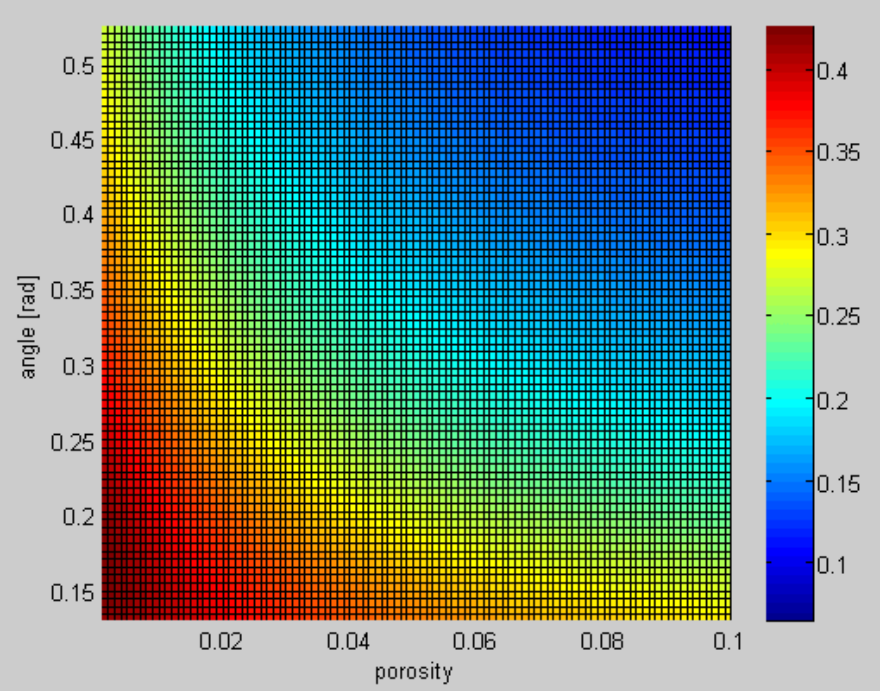

Figure 3.8. Averaged absorption coefficient in 500 to 10000 Hz (porosity vs. angle).

Figure 3.8 shows the trend of averaged absorption coefficient in the 500 to 10000 Hz range (when the radius of the inlet hole was 0.0001 m, the thickness of the panel was 0.0004 m, and the mass per unit area was 1 kg/m^2), that results from changing the angle of the hole and the porosity simultaneously. These result show that there is a trade-off between the angle of the hole and porosity. This implies that it is possible to achieve the same performance with a small number of holes on the microperforated panel. Figure 3.9 shows the relation between angle and porosity when the averaged absorption coefficient has a constant value.

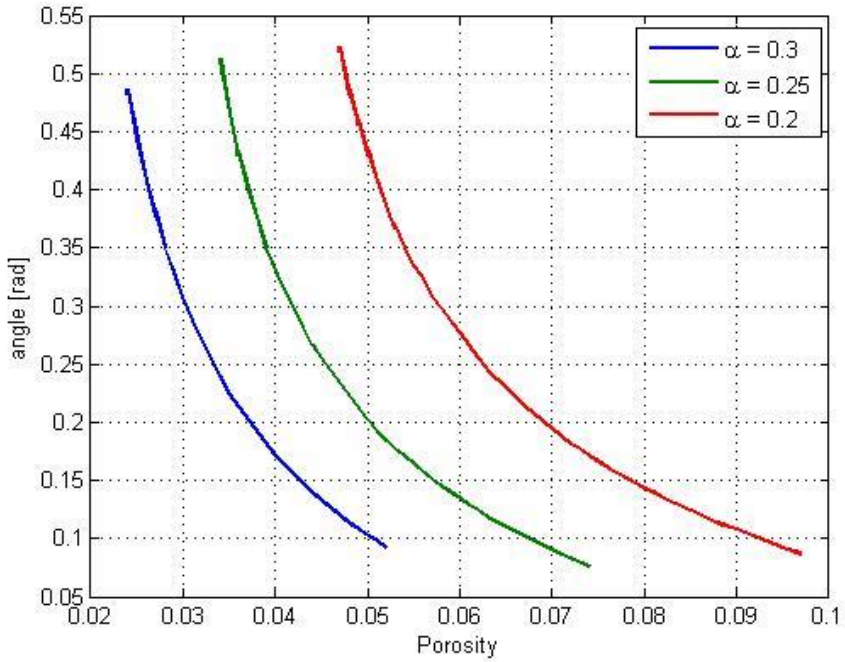

Figure 3.9. Relation between angle and porosity when the averaged absorption coefficient is constant.

For the curve fitting, a third degree polynomial was used, and equations can be expressed as:

$$\theta_{\alpha=0.3} = -21790\sigma_{\alpha=0.3}^3 + 2976\sigma_{\alpha=0.3}^2 - 141.5\sigma_{\alpha=0.3} + 2.462 \quad (3.7)$$

$$\theta_{\alpha=0.25} = -11680\sigma_{\alpha=0.25}^3 + 2188\sigma_{\alpha=0.25}^2 - 140.2\sigma_{\alpha=0.25} + 3.193 \quad (3.8)$$

$$\theta_{\alpha=0.2} = -5812\sigma_{\alpha=0.2}^3 + 1439\sigma_{\alpha=0.2}^2 - 141.7\sigma_{\alpha=0.2} + 3.653\ . \quad (3.9)$$

To formulate the equation for a general case, all constants were fitted with all th absorption coefficients considered. And the result was:

$$\theta = a_1\sigma^3 + a_2\sigma^3 + a_3\sigma + a_4 \quad (3.10\text{-a})$$

$$a_1 = -8.5 \times 10^5\alpha^2 + 2.6 \times 10^5\alpha - 2.5 \times 10^4 \quad (3.10\text{-b})$$

$$a_2 = 1.54 \times 10^4\alpha - 1640 \quad (3.10\text{-c})$$

$$a_3 = 140.6 \quad (3.10\text{-d})$$

$$a_4 = -11.9\alpha + 6.08. \quad (3.10\text{-e})$$

Three different sets of results, which all have an averaged absorption coefficient of 0.3, are plotted in Figure 3.10, calculated based on Equation (3.10) These results show that a panel having a small porosity, but larger taper angle gives, on average, the same performance as a panel with a porosity nearly twice as large but with a relatively small taper angle

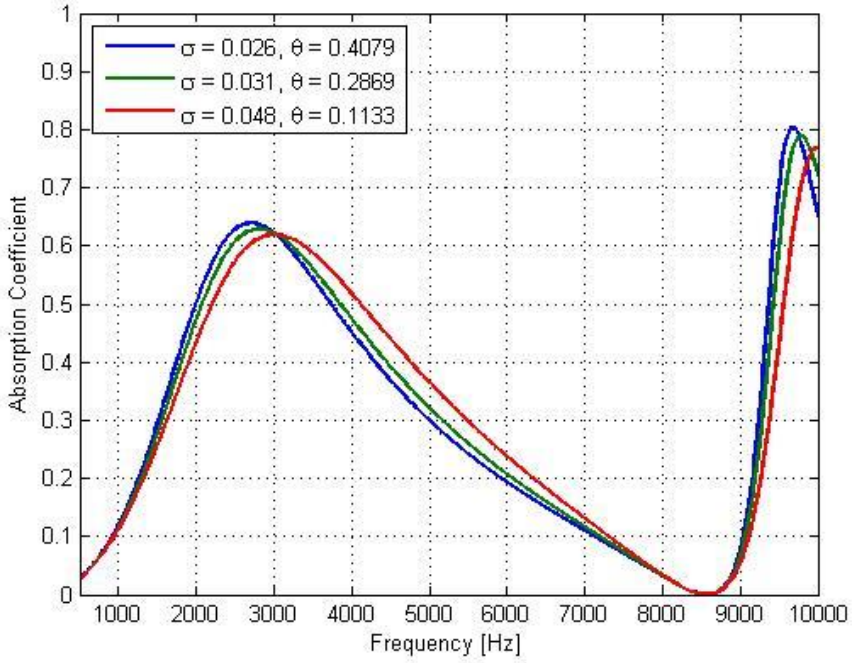

Figure 3.10. Absorption coefficient of 3 different sets of tapered hole MPPs.

3.3 Optimization

Given the above findings, the identification of an optimal set of panel parameters was considered next. The limit on the panel parameters were: diameter of inlet hole, 0.0001 to 0.0004 m; thickness of panel, 0.0001 to 0.001 m; porosity, 0.001to 0.1; perforation angle, 0° to 30 °; and mass per unit area, 0.5 to 1.5 kg/m^2. The genetic algorithm was used for the optimization, and the error function was set as $\sum(1-\alpha)$ over the frequency range 500 to 10000 Hz.

3.4 Result

The result of the optimization is shown in Table. 3.1. From the optimization results, it can be seen that the thickness of the panel and mass per unit area are

maximized, and the inlet hole radius is minimized. Note that if the upper or lower boundary of constraints were changed, then the thickness of the panel goes to its higher limit and the diameter of hole goes to its lower limit. But the constraints of the optimization, used in here, were chosen because these limits were widely used in the commercial area. Figure 3.11 shows the absorption coefficient of the system. The absorption coefficient has a peak at about 2500 Hz. However the bandwidth of peak is slightly more than two octaves.

Table 3.1. The optimization result of single tapered hole microperforated panel with air depth D =0.02 m.

Thickness [m]	Diameter [m]	Porosity	Angle of hole [degree]	Mass per unit area [kg/m^2]
0.001	**0.0001**	0.01376	0.9998	**1.5**

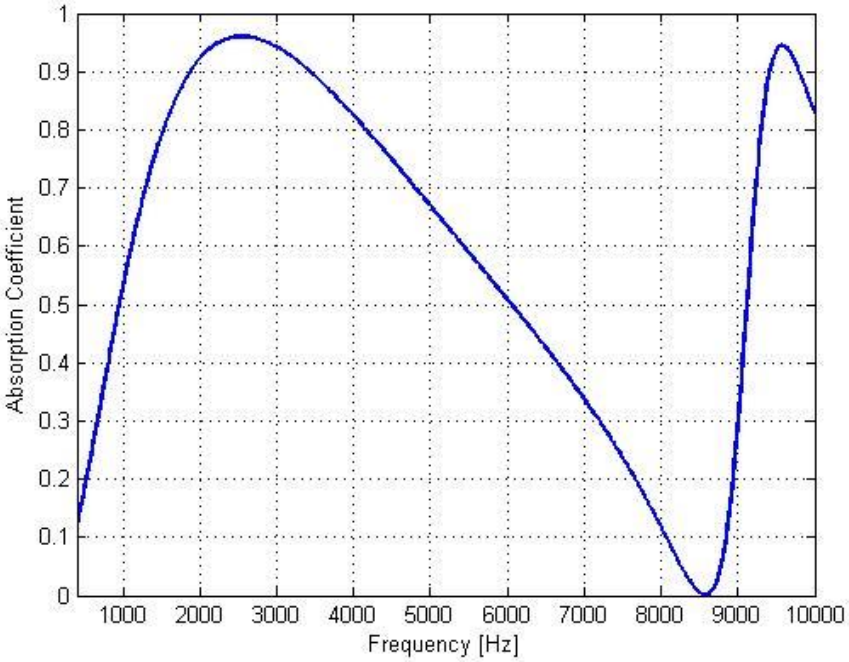

Figure 3.11. Absorption coefficient of optimal design of tapered hole MPP.

3.5 Summary

The performance of a microperforated panel with tapered holes is determined by the radius of hole, thickness, porosity, angle, and mass per unit area. It has been shown here that the angle of the hole and porosity can be traded-off, and that a larger hole angle can give excellent performance at a relatively small porosity. In addition, the optimization result shows that the proper combination of parameters can result in a high performance solution, but where the absorption is limited in bandwidth. The use of multiple layers is necessary to increase the band width of the absorption offered by microperforated panels, and the modeling of that case is considered in the next chapter.

CHAPTER 4. TRANSFER MATRIX MODELING OF MULTI-LAYER MICROPERFORATED PANELS

In the following chapters of this thesis, the optimal design of multi-layer microperforated panel systems will be considered in various contexts. In all cases, the systems have been modeled by using a transfer matrix approach that relates the sound pressure and particle velocity on two sides of an acoustic element. The implementation of that modeling strategy is described in this chapter.

4.1 Transfer Matrix Method

The transfer matrix method is a very effective tool for calculating the absorption coefficient and transmission loss for one-dimensional acoustical systems (Song and Bolton, 1999). The pressure and normal velocity at the two faces of the acoustical system can be related by a 2-by-2 transfer matrix as:

$$\begin{bmatrix} P_1 \\ u_1 \end{bmatrix} = \begin{bmatrix} TM_{11} & TM_{12} \\ TM_{21} & TM_{22} \end{bmatrix}_{total} \begin{bmatrix} P_2 \\ u_2 \end{bmatrix} = [\mathrm{TM}]_1[\mathrm{TM}]_2[\mathrm{TM}]_3 \cdots [\mathrm{TM}]_\mathrm{n} \begin{bmatrix} P_2 \\ u_2 \end{bmatrix} \tag{4.1}$$

where $[\mathrm{TM}]_1$, etc., represent the transfer matrices of a series of acoustic elements, either microperforated panels or air spaces in the current work.

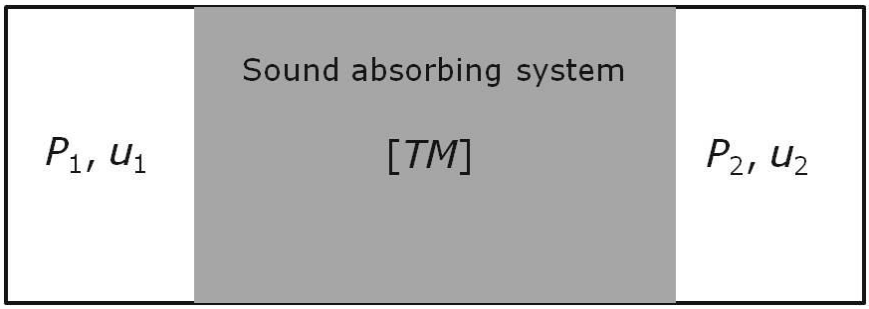

Figure 4.1. Transfer matrix with four parameters.

After assuming appropriate forms for the incident and transmitted sound fields, the plane wave reflection, Γ, and transmission coefficients, τ, can expressed in terms of the transfer matrix elements as

$$\Gamma = \frac{TM_{11}^{total}+TM_{12}^{total}(\cos\theta/\rho c)-(\rho c/\cos\theta)TM_{21}^{total}-TM_{22}^{total}}{TM_{11}^{total}+TM_{12}^{total}(\cos\theta/\rho c)+(\rho c/\cos\theta)TM_{21}^{total}+TM_{22}^{total}} \tag{4.2}$$

$$\tau = \frac{2e^{j\frac{\omega L}{c}\cos\theta}}{TM_{11}^{total}+TM_{12}^{total}(\cos\theta/\rho c)+(\rho c/\cos\theta)TM_{21}^{total}+TM_{22}^{total}} \tag{4.3}$$

where ω is the angular frequency, c is the speed of sound, ρ is the air density, L is the total treatment depth, and θ is the incident angle (θ=0 is the normal incidence case). Further, a dissipation coefficient (i.e., the fraction of the incident energy that is neither reflected nor transmitted and so is dissipated within the system) can be expressed, as

$$\alpha_d = 1 - |\Gamma|^2 - |\tau|^2. \tag{4.4}$$

The transmission loss of the system, in decibels is

$$TL = 10\log(\frac{1}{|\tau|^2}). \tag{4.5}$$

And the dissipation coefficient for random incidence sound fields is

$$\overline{\alpha_d} = \frac{\int_0^{\pi/2} \alpha_d(\theta) \sin(\theta) \cos(\theta) d\theta}{\int_0^{\pi/2} \sin(\theta) \cos(\theta) d\theta}, \tag{4.6}$$

while the random incidence power transmission coefficient is calculated as

$$\bar{\tau} = \frac{\int_0^{\pi/2} |\tau(\theta)|^2 \, sin(\theta) \, cos(\theta) d\theta}{\int_0^{\pi/2} sin(\theta) \, cos(\theta) d\theta} \, . \tag{4.7}$$

From the latter expression, the random incidence transmission loss can be calculated as $\overline{TL} = 10 \log_{10}(1/\bar{\tau})$.

To evaluate Eqs. (4.4) and (4.5), the transfer matrix for each layer in the multilayer system is needed. In this thesis, two layer types are considered: one is for air layers, and the other is for microperforated panels.

For a locally reacting air space of depth l, the transfer matrix (Lai et al., 1997) can be expressed as:

$$[TM]_{air} = \begin{bmatrix} cos\ (\omega l/c) & j\rho c sin(\omega l/c) \\ (j/\rho c) sin\ (\omega l)/c) & cos\ (\omega l/c) \end{bmatrix} \tag{4.8}$$

where ω is the angular frequency, c is the speed of sound, ρ is the air density, and the air layer between the panels is assumed to be segmented, and so to be locally reacting.

For a microperforated panel (Lai et al., 1997), the transfer matrix is

$$[TM]_{mpp} = \begin{bmatrix} 1 & Z_{mpp} \\ 0 & 1 \end{bmatrix} \tag{4.9}$$

where Z_{mpp} is the transfer impedance of a microperforated panel. The transfer impedance of a MPP, as expressed in the Maa model, can be separated into two parts, one being a linear component and the other being a non-linear component which becomes significant at high incident sound pressure levels. In this study, the focus is on the linear part, only. The linear component of the Maa model is derived from Rayleigh's formulation for wave propagation in narrow tubes which was further developed by Crandall. Maa then applied Crandall's model to the case of very small holes in which the oscillatory viscous boundary layer spans the hole. According to the Maa model, the normal transfer impedance of a microperforated sheet (without end corrections), is expressed as:

$$z = \frac{j\omega t}{\sigma c}\left[1 - \frac{2}{k\sqrt{-j}}\frac{J_1(k\sqrt{-j})}{J_2(k\sqrt{-j})}\right]^{-1} \tag{4.10}$$

where t is the length of the hole (usually the same as the thickness of the perforated sheet), σ is the surface porosity of the sheet (i.e., the fraction of the surface area occupied

by holes), k is the perforation constant defined by $k = d\sqrt{\omega\rho/4\eta}$, η is the dynamic viscosity, d is the hole diameter, and J_0 and J_1 are the Bessel functions of the first kind of zeroth and first order, respectively.

A resistive end correction was suggested by Ingard, to account for energy dissipation at the surface of the sheet as flow approaches the hole. Ingard called this effect a surface resistance, and the surface resistance on one side of the hole was defined as $R_s = \frac{1}{2}\sqrt{2\eta\rho\omega}$. In the microperforated panel formulation of Guo et al., the end correction is added to the real part of the above expression as:

$$r = \mathrm{Re}\left\{\frac{j\omega t}{\sigma c}\left[1 - \frac{2}{k\sqrt{-j}}\frac{J_1(k\sqrt{-j})}{J_2(k\sqrt{-j})}\right]^{-1}\right\} + \frac{\alpha 2R_s}{\sigma\rho c} \tag{4.11}$$

where r is the real part of the specific acoustic impedance, R_s is the surface resistance, and α is a nominally frequency-independent factor which accounts for hole type. It was suggested by Guo et al., based on a comparison with measurements, that α should be set to 4 when the hole is sharp-edged. However, in previous work (Kim and Bolton, 2012), it was found that α needs to be made a function of frequency, and that α can be expressed as:

$$\alpha = (16.9\frac{t}{d} + 152.8)f^{-0.5} \tag{4.12}$$

In this thesis, Eqs. (4.11) and (4.12) were used to calculate the resistance of the MPP. However, the above equation does not consider the flexural movement of the MPP. In that case, a velocity continuity equation and force equilibrium equations are needed for calculating Z_{mpp}. (Yoo, 2008) When it is assumed that the MPP is a limp panel (which means that its flexural stiffness is negligible) then the continuity, and equilibrium equations for the solid and fluid components are, respectively,

$$v_y = (1-\sigma)v_s + \sigma v_f \tag{4.13}$$

$$P_1 - P_2 + (v_f - v_s)R\frac{\sigma^2}{1-\sigma} = j\omega m \mathrm{v_s} \tag{4.14}$$

$$P_1 - P_2 + (v_f - v_s)R\sigma = \rho h_p j\omega \mathrm{v_f} \tag{4.15}$$

where v_y is the normal particle velocity, v_s is the velocity of the solid part of the panel, v_f is the velocity of the fluid part of the panel, P_1 and P_2 are the acoustic pressures on the front and rear surfaces of the panel, $R = \rho cr$ is the flow resistance of the panel, m is the mass per unit area of the panel, $h_p = t + 2\delta$ is the effective hole depth of the panel, and $\delta = 8d/3\pi$. Finally, the impedance of the flexible MPP can be defined as (Yoo, 2008)

$$Z_{mpp} = \frac{R\sigma(1-\sigma)(j\omega m - j\omega\rho(t+2\delta)) + j\omega\rho(t+2\delta)\{j\omega m(1-\sigma)+R\sigma\}}{\sigma(1-\sigma)(R+j\omega m)+(1-\sigma)^2\rho(t+2\delta)j\omega+\sigma^2 R} \quad . \tag{4.16}$$

4.2 Optimization

In the work described in this thesis, optimization of multilayer MPP systems for the dissipation coefficient, or the transmission loss, or for joint properties, was performed over the speech interference range. In these multilayer panel sound absorbing systems, there are two different kinds of layers, as shown in Fig. 4.2: one is the locally reacting air space layer, and the other is the MPP layer.

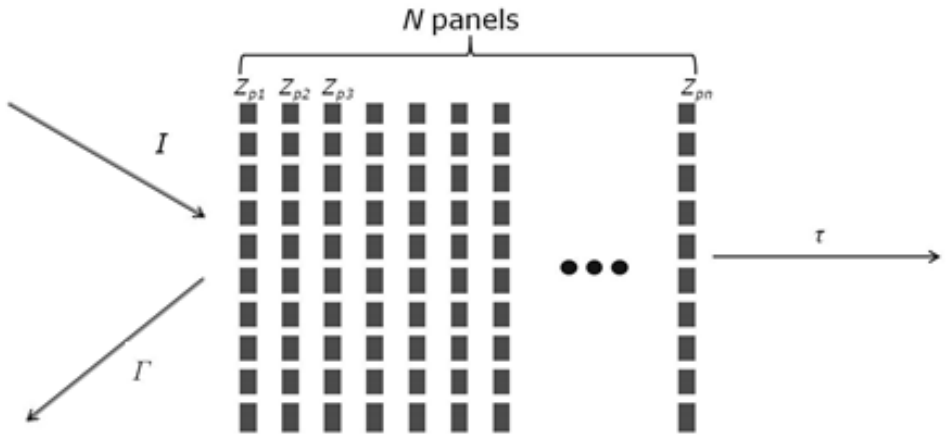

Figure 4.2. *N* layers of microperforated panels.

The transfer matrix of the air space layers is determined by the distance between the panels, and the transfer matrix of the MPP is defined by its thickness, the hole diameter, porosity, and the mass per unit area. Since Eq. (4.12) was verified in the range 0.2 to 0.8 mm for thickness, 0.1 to 0.3 mm for hole diameter, and 0.01 to 0.2 for porosity, the range of parameter variation in the various optimization was accordingly limited, as shown in Table 4.1. These limits apply in the various cases discussed from Chapters 5 to 8. Note that *L* is the total thickness of the multilayer arrangement, and *M* is total mass

per unit area of the multilayer system. From a practical point-of-view, if the total thickness L is too thick or if total mass per unit area M is too heavy, then a multilayer MPP system is no more beneficial than other sound absorbing systems.

Table 4.1. Constraints of components.

	Minimum	Maximum
N	2	10
t [mm]	0.2	0.8
d [mm]	0.1	0.3
σ	0.01	0.2
m [kg/m^2]	0.1	0.8
l [m]	0.001	0.2
M [kg/m^2]		3
L [m]		0.5

Note that the dissipation coefficient was calculated for waves striking both the front and rear surfaces of the assembly. The transmission loss has the same value for sound coming from either direction, but the dissipation coefficient can differ with direction of incidence, so here, the dissipation coefficients for the two different cases were averaged. For the optimization, a genetic algorithm was used, and it was focused on the 500 Hz to 4000 Hz range. To provide a basis for comparison with the optimized results, combinations of parameters were created with the same distances between the panels as in the optimized cases but with uniform panel properties. To maximize the flow resistance of each panel, and so to create the so-called “maximum resistances” case, the maximum values were chosen for thickness and mass per unit area, and the minimum values were chosen for porosity and hole diameter (see Table 4.2).

Table 4.2. Maximum resistance set.

t [mm]	0.8
d [mm]	0.1
σ	0.01
m [kg/m^2]	3/N
l [m]	0.5/N
M [kg/m^2]	3
L [m]	0.5

4.3 Summary

In this chapter, the approach to modeling the acoustic performance of multi-layer microperforated panel has been reviewed, along with the acoustic properties of single microperforated panels. This modeling approach is used throughout Chapters 5 to 8. And to support the optimization, the limits on each parameter of the microperforated panels, were defined. And finally, a maximum resistance set was chosen for comparison with optimization results presented in chapters 5 to 8.

CHAPTER 5. FUNCTIONAL ABSORBER

A functional absorber usually hangs from the ceiling or is attached to a wall, and the main purpose of a functional absorber in acoustics is to dissipate acoustic energy in a space. Usually, a functional absorber covers a broad range of frequencies, the audible range or speech interference range, for example, and so are composed with different types of sound absorbing materials. If it is possible to replace these sound absorbing materials with multi-layers of microperforated panels, then functional absorbers can potentially be much lighter.

5.1 Optimization

To see the trend of the acoustic properties of functional absorbers, two layer microperforated panels systems were considered. One MPP was fixed with standard parameters and only one parameter at a time of the other MPP was varied from the standard parameters. The standard parameters of the microperforated panels were: the radius of inlet hole is 0.0001 m, thickness of the panel is 0.0004 m, the porosity is 0.02, mass per unit area is 0.3 kg/m^2, and air space between two panels is 0.3 m. Figures 5.1 to 5.5 show the trend of the dissipation coefficient by changing each parameter in turn: thickness of panel, hole diameter, porosity, mass per unit area, and air space between two panels. As shown in the figures, if the panel is thin enough or the porosity is low enough

or the mass per unit area is large enough, then the dissipation coefficient is increased. For the hole diameter, a specific hole diameter (here, d = 0.15 mm) makes the dissipation coefficient a maximum. And the peak location and bandwidth of the dissipation coefficient depends on the air space between the panels, as shown as Figure 5.5.

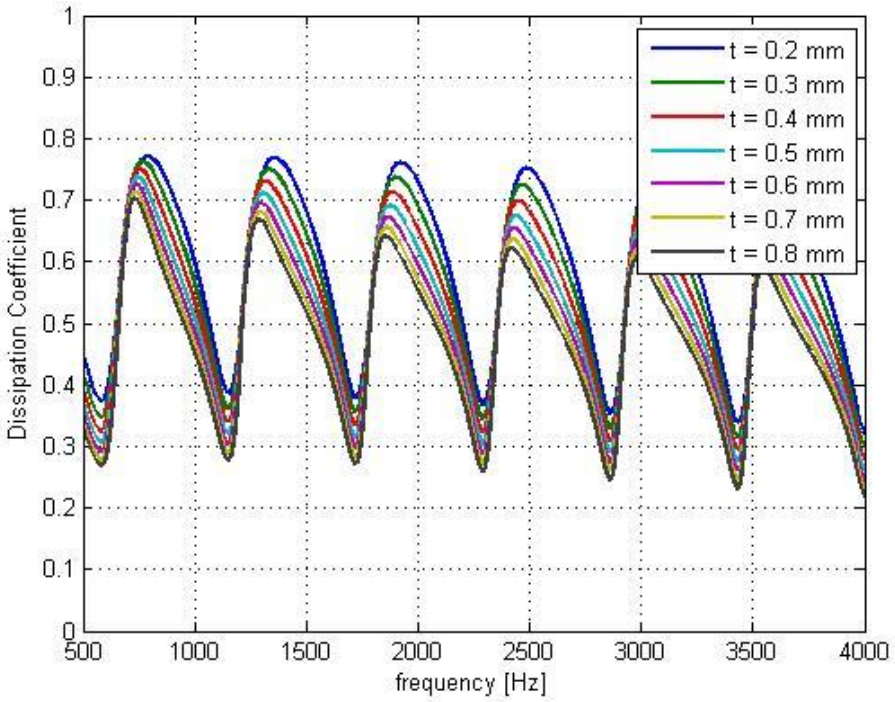

Figure 5.1. Dissipation coefficient of double layer microperforated panel system by change of thickness.

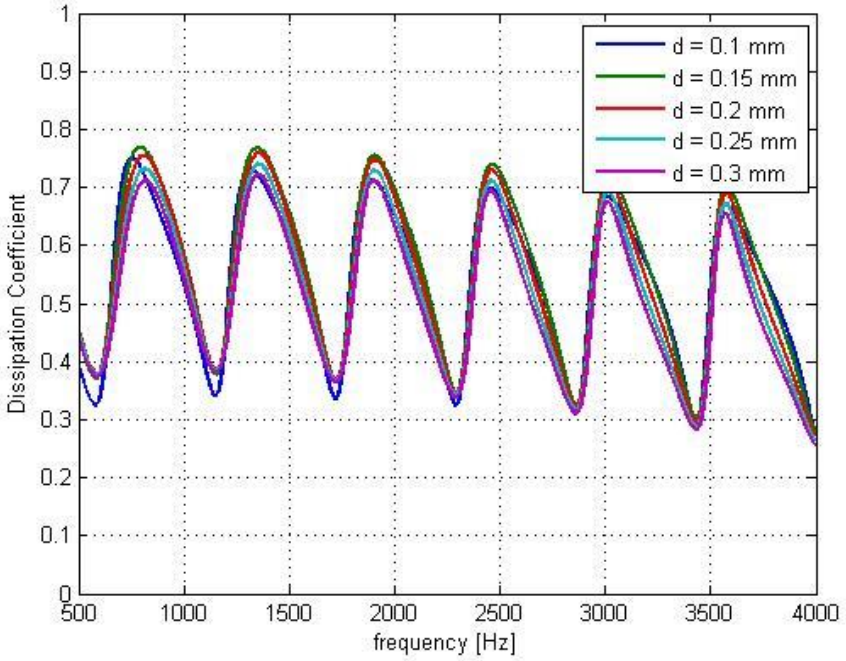

Figure 5.2. Dissipation coefficient of double layer microperforated panel system by change of diameter of hole.

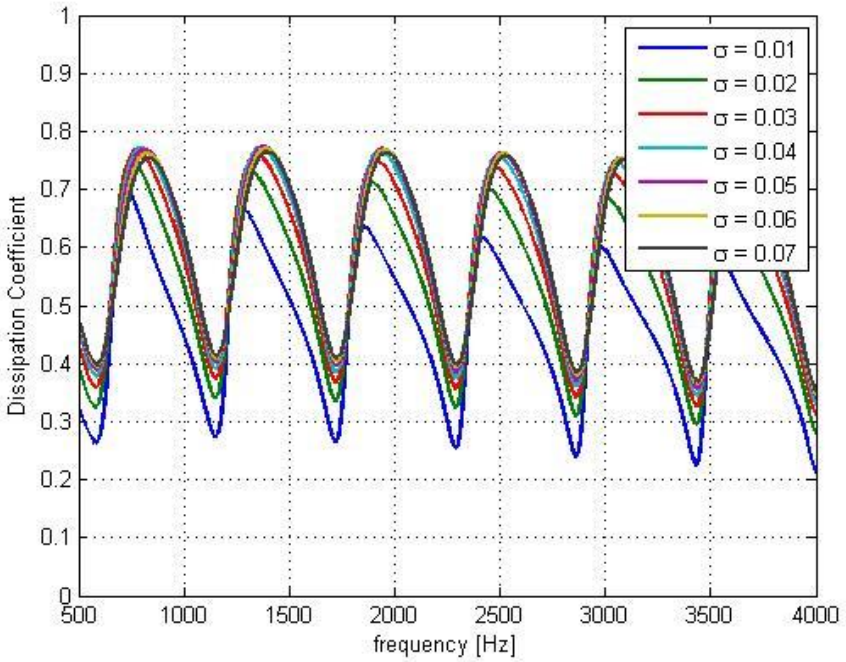

Figure 5.3. Dissipation coefficient of double layer microperforated panel system by change of porosity.

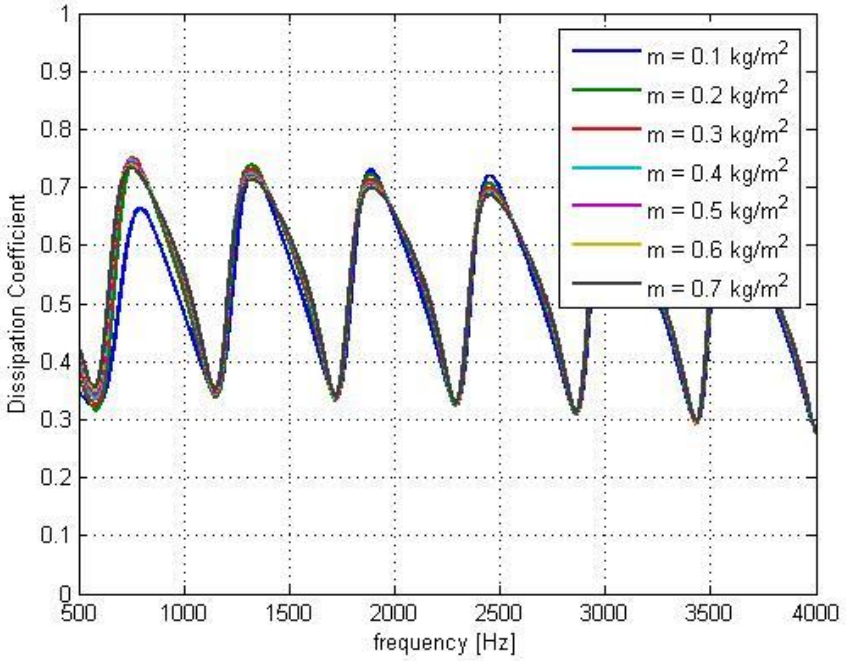

Figure 5.4. Dissipation coefficient of double layer microperforated panel system by change of mass per unit area.

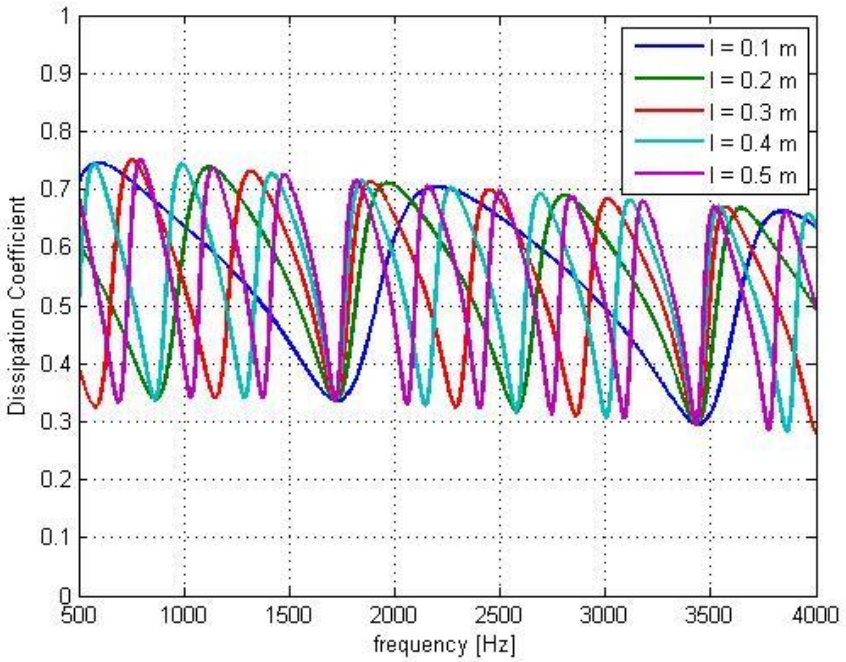

Figure 5.5. Dissipation coefficient of double layer microperforated panel system by change of air space.

The main purpose of a functional absorber is to absorb sound in specific frequency range, so the dissipation coefficient of the system is the focus of the optimization performed here. In this case, both directions of dissipation coefficients were considered, and the objective of the optimization was to maximize the dissipation coefficient, so the error function was set as $\sum 1 - \alpha_d$. Two different cases, the normal and random incidence cases, were considered in this work.

5.2 Normal Incidence

The optimization for the normal incidence functional absorber case was calculated by using the genetic algorithm, and Figure 5.6. is the optimization result for different numbers of panels.

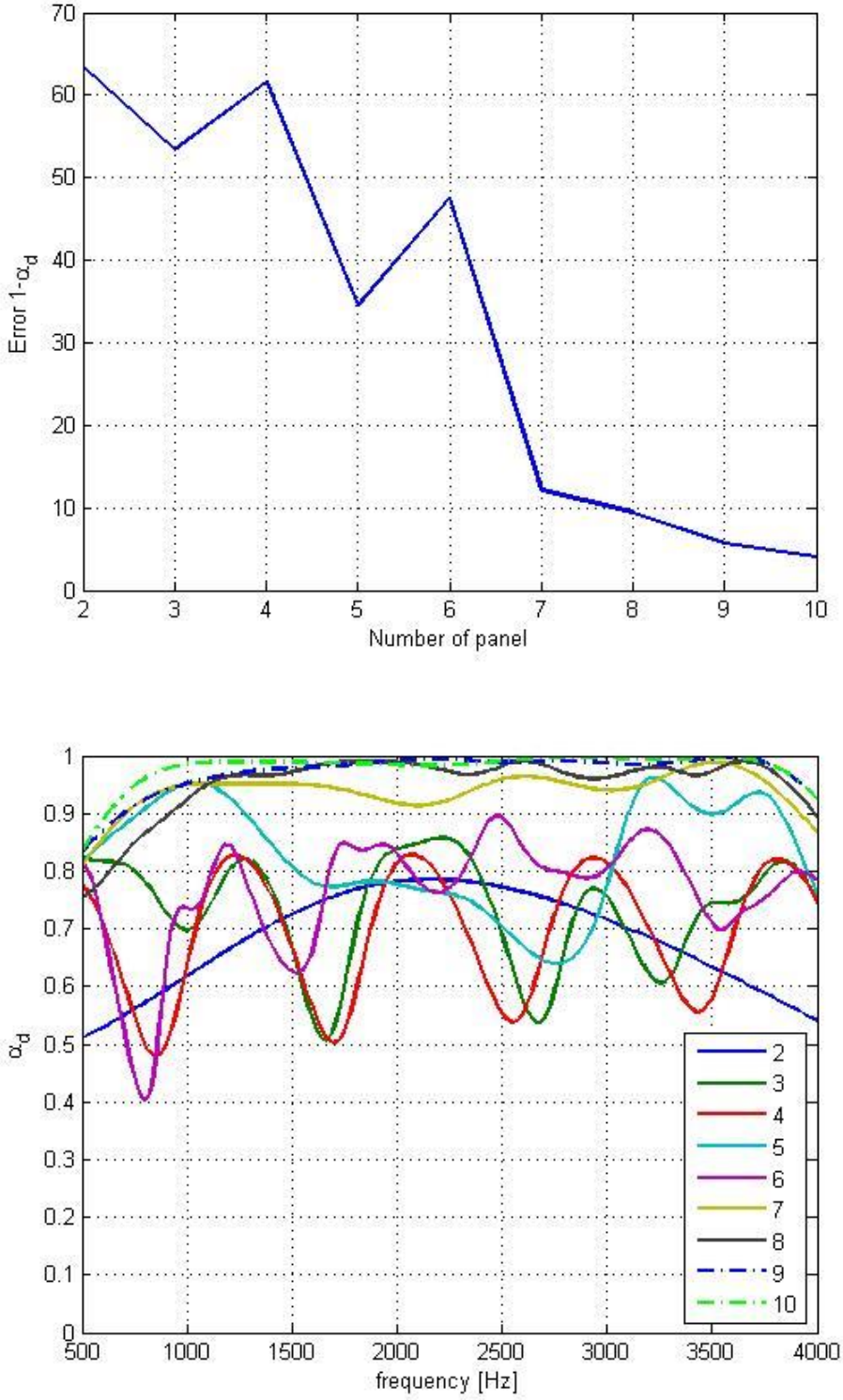

Figure 5.6. Optimization results by number of panels for normal incidence functional absorber.

From Figure 5.6, the functional absorber with 10 panels was chosen as the best and Table 5.1. gives the properties of the functional absorber system. Bold letter in Table 5.1 indicates that a parameter is on its upper or lower limit.

Table 5.1. Optimized set for a functional absorber in normal incidence case.

	Thickness [mm]	**Diameter [mm]**	**Porosity**	**Mass per unit area [kg/m^2]**	**Distance to next panel [m]**
Panel 1	0.574	**0.300**	0.129	0.106	0.021
Panel 2	0.482	0.102	0.138	0.134	0.019
Panel 3	0.427	**0.300**	0.169	0.117	0.019
Panel 4	**0.800**	**0.300**	0.047	0.148	0.017
Panel 5	**0.800**	**0.100**	0.076	0.387	0.034
Panel 6	0.799	**0.100**	0.041	0.312	0.048
Panel 7	**0.800**	**0.100**	0.091	0.654	0.026
Panel 8	0.501	0.126	0.080	0.391	0.041
Panel 9	0.505	**0.100**	0.142	0.480	0.022
Panel 10	**0.800**	**0.300**	0.155	0.253	-

As shown in Figure 5.7., the dissipation coefficient of the optimized set is much higher overall in the speech interference range than that of the maximum resistance set.

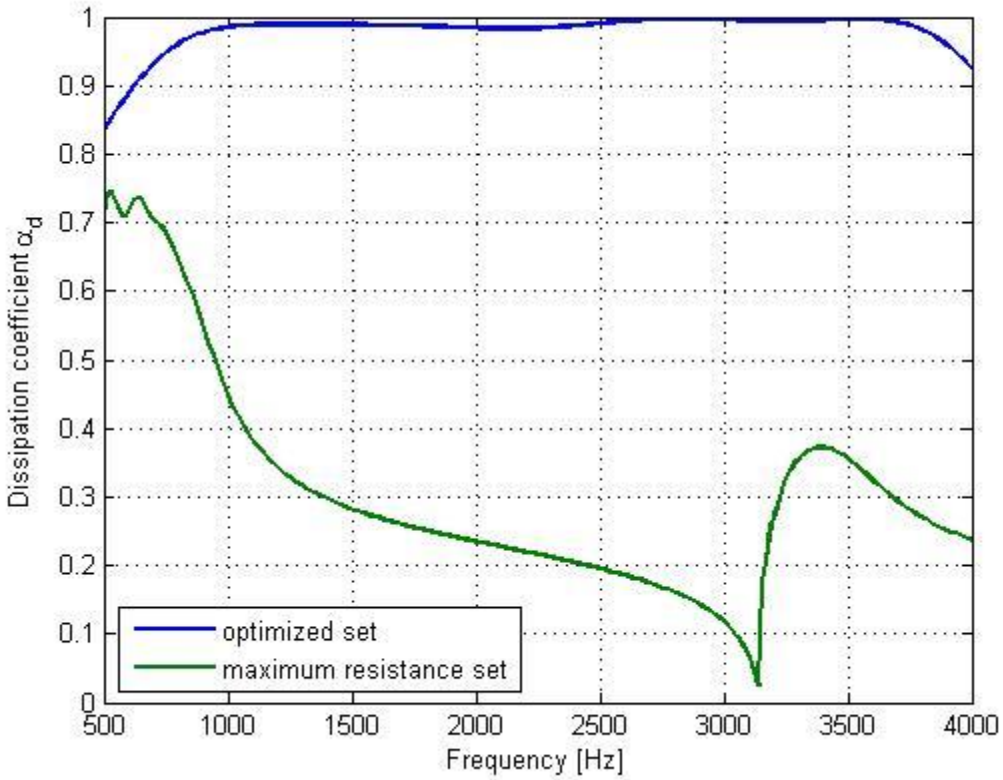

Figure 5.7. Comparison of optimized set for normal incidence functional absorber case with maximum resistance set (10 panels).

5.3 Random Incidence

As before, the optimization for the random incidence functional absorber case was performed by using the genetic algorithm and only the local reaction case was considered. Figure 5.8. is the optimization result for different numbers of panels. From Figure 5.8, the system with 9 panels appears to be the best, so the functional absorber with 9 panels was chosen and Table 5.2. is the result of the optimization.

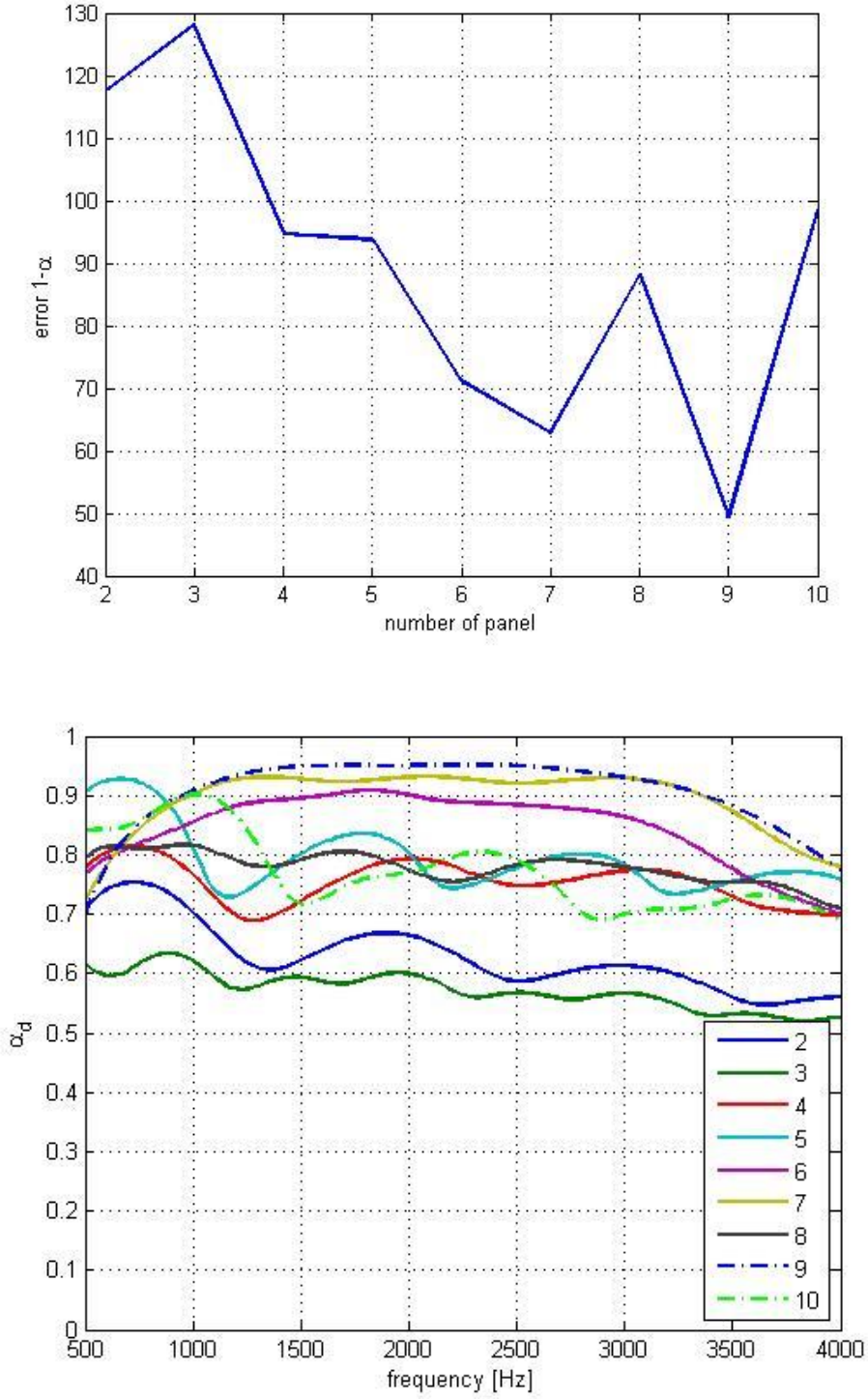

Figure 5.8. Optimization results by number of panels for random incidence functional absorber.

Table 5.2. Optimized set for a functional absorber in random incidence case.

	Thickness [mm]	Diameter [mm]	Porosity	Mass per unit area [kg/m^2]	Distance to next panel [m]
Panel 1	0.341	0.283	0.064	0.697	0.037
Panel 2	0.735	0.119	0.061	0.118	0.040
Panel 3	0.753	**0.100**	0.065	0.229	0.037
Panel 4	0.678	**0.100**	0.024	0.709	0.005
Panel 5	0.749	**0.300**	0.044	0.731	0.037
Panel 6	0.796	**0.100**	0.044	0.188	0.018
Panel 7	0.444	**0.300**	0.013	0.112	0.040
Panel 8	0.796	0.161	0.122	0.105	0.029
Panel 9	0.749	**0.300**	0.073	0.100	-

In Figure 5.9., as in the normal incidence case, the optimized set shows much better overall performance than the maximum resistance set in the speech interference range.

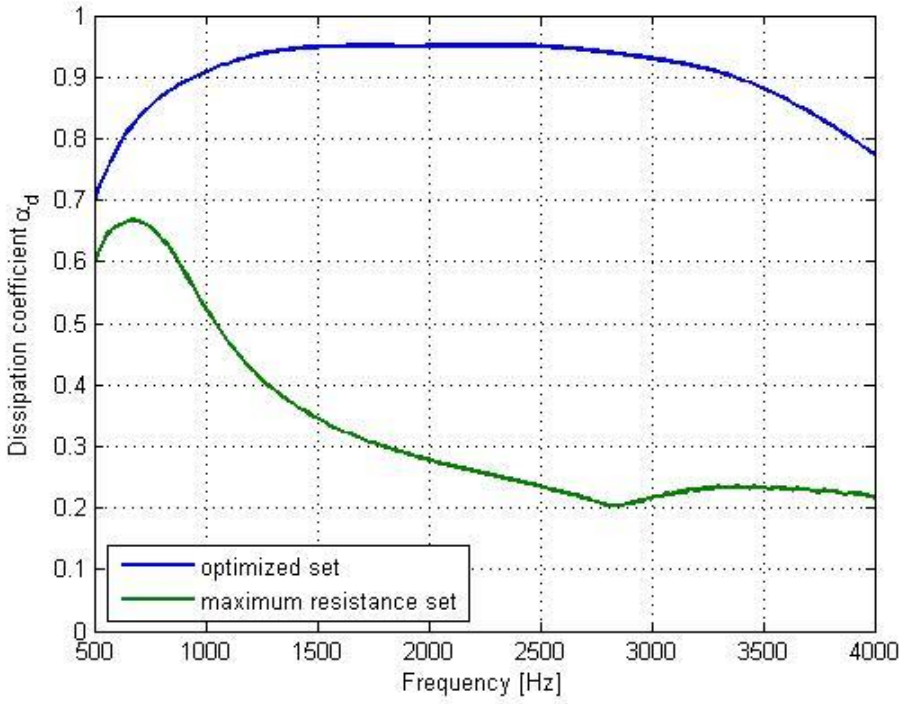

Figure 5.9. Comparison optimized set for random incidence functional absorber case with maximum resistance set (9 panels).

5.4 Summary

In this chapter, a functional absorber for the normal and random incidence cases was discussed. Based on the result, it has been shown that an appropriate combination of microperfoated panels can provide excellent performance for sound absorption. This suggests that a layered array of MPPs proper could be used to provide acoustic energy dissipation in a space: i.e., the array could be used as a functional absorber. As mentioned before, multi-layer microperforated panel systems could replace the fiberglass, material that is now used for functional absorbers, to make an eco-friendly environment. And also, an appropriate combination of microperforated panels makes a much lighter system than we use now.

CHAPTER 6. BARRIER

A barrier, also called a soundwall, or acoustic barrier, is used to protect people from noise source areas, such as roadways, railways, and industrial noise sources. The main function of a barrier in acoustics is to block the noise from a source transmitting to the other side of the barrier. Usually, to block noise perfectly, a heavy and thick wall is needed. But if multi-layers of microperforated panels can provide a high enough transmission loss, then the heavy barrier might potentially be replaced with lighter systems.

6.1 Optimization

To see the trend of the acoustic properties of barriers, two layers microperforated panels system were considered. As for the functional absorber case, one MPP was fixed with standard parameters and only one parameter of the other MPP was varied at a time from standard parameters. The standard parameters of the microperforated panel were: the radius of inlet hole is 0.0001 m, the thickness of the panel is 0.0004 m, the porosity is 0.02, the mass per unit area is 0.3 kg/m^2, and air space between the two panels is 0.3 m. The trend of transmission loss obtained by varying each parameter, which is the thickness of panel, hole diameter, porosity, mass per unit area, and the air space between the two panels, are shown in Figures 6.1 to 6.5. As shown in the figures, if the panel is thick

enough or the porosity is low enough or the hole diameter is small enough or the mass per unit area is large enough, then the transmission loss is increased. And, as for the dissipation coefficient, the air space between the panels determines peak location and bandwidth of the transmission loss as shown as Figure 6.5.

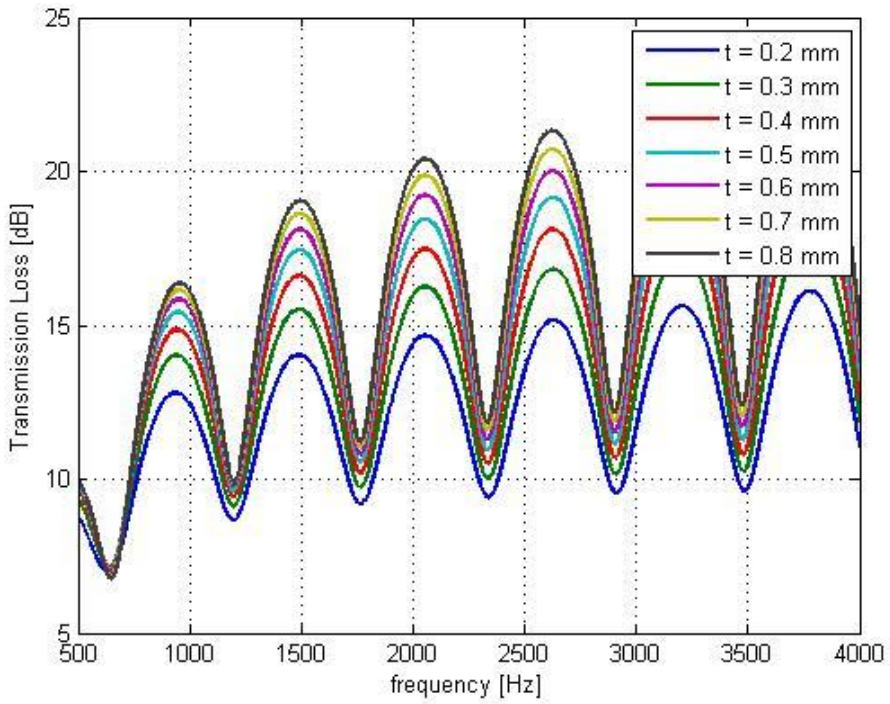

Figure 6.1. Transmission loss of double layer microperforated panel system by change of thickness.

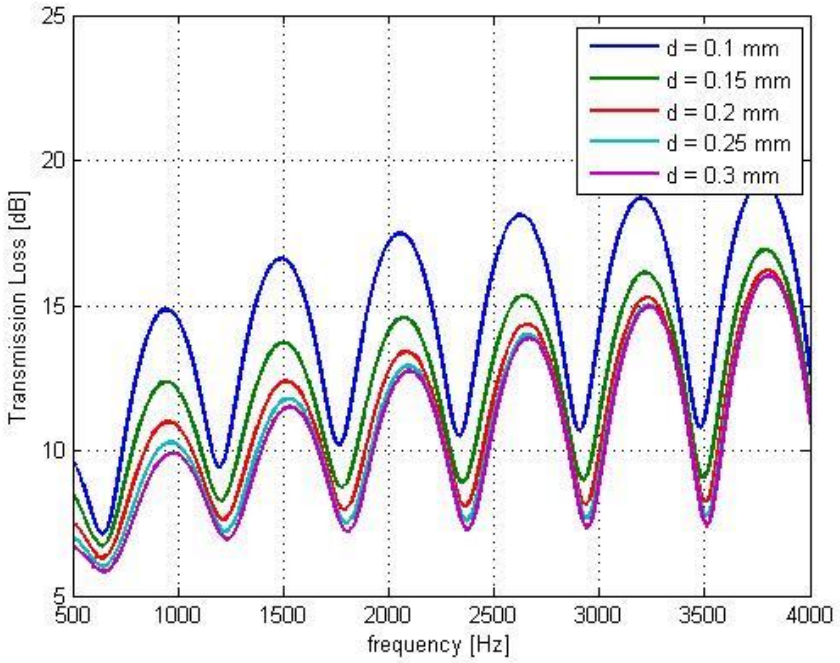

Figure 6.2. Transmission loss of double layer microperforated panel system by change of diameter of hole.

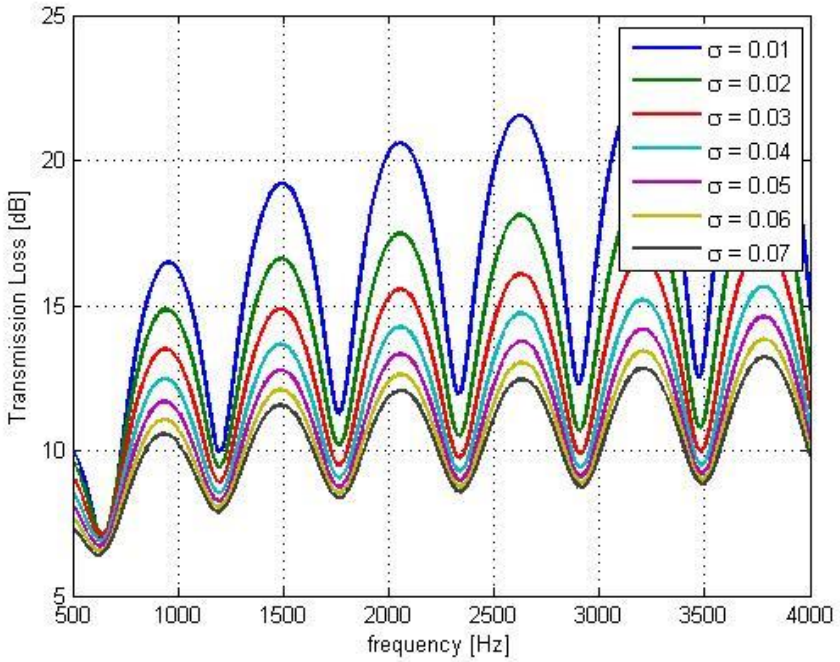

Figure 6.3. Transmission loss of double layer microperforated panel system by change of porosity.

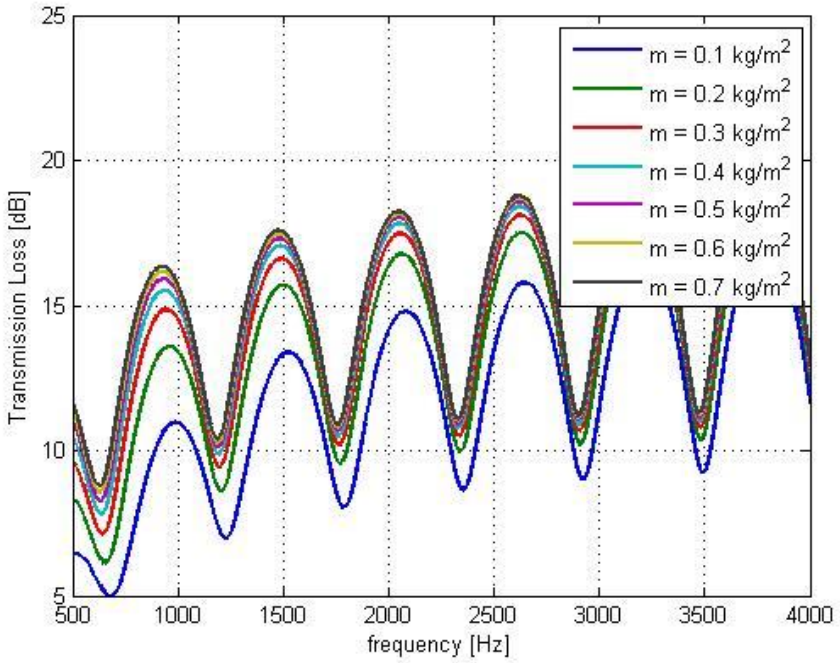

Figure 6.4. Transmission loss of double layer microperforated panel system by change of mass per unit area.

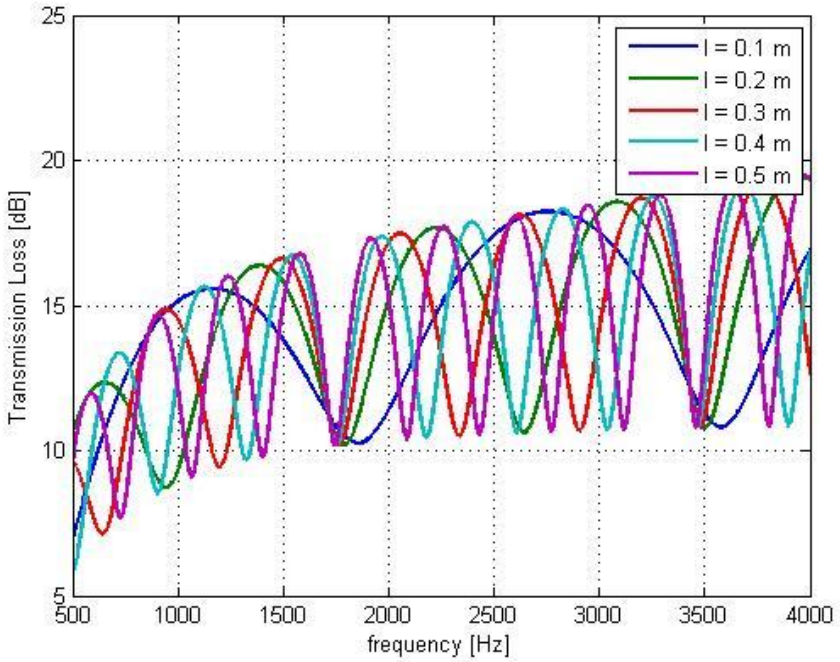

Figure 6.5. Transmission loss of double layer microperforated panel system by change of the air space.

The objective of the optimization for a barrier is to maximize the transmission loss in order to block the noise as much as it can, and also to eliminate resonances in the frequency range of interest to avoid passing all of the noise at a specific frequency. To satisfy these two conditions, the error function was set as $\sum 1/TL$. This is a one-direction calculation, since the transmission loss in either direction is the same.

6.2 Normal Incidence

First, consider the normal incidence case. The normal incidence case means that sound passes through the multi-layer MPP only in the normal direction. As mentioned earlier, the genetic algorithm method was used for the optimization, and 1/*TL* was used for the error function. Figure 6.6. is the result of optimization as a function of the number of panels. Fig. 6.6(a) shows the change of error by number of panels and Fig. 6.6(b) is for comparison of the optimization result by changing number of panels. From Figure 6.6, 5 panels were chosen for the optimized barrier for normal incidence and Table 6.1 shows the properties of the optimized set.

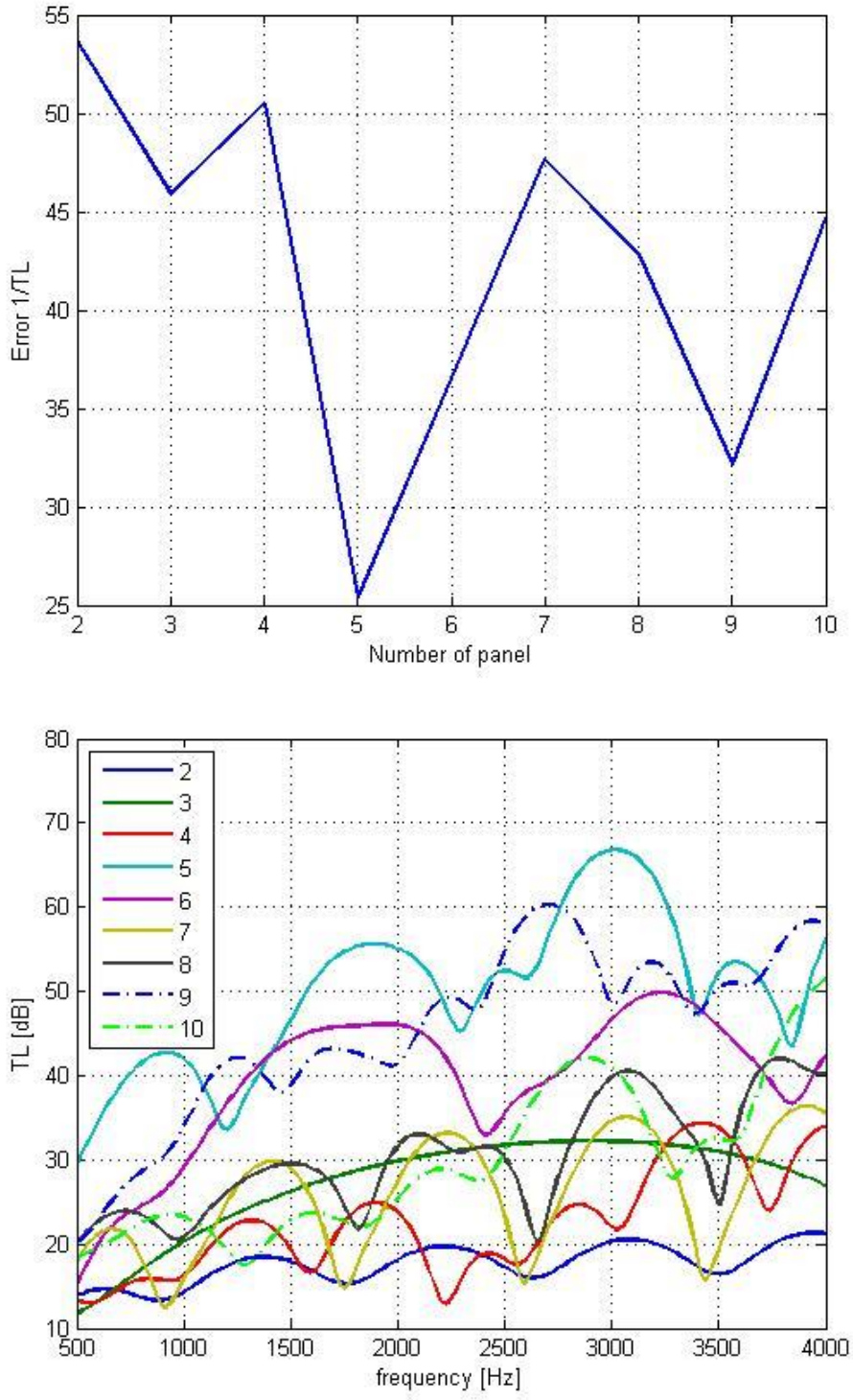

Figure 6.6. Optimization results by number of panels for normal incidence barrier.

Table 6.1. Optimized set for a barrier in normal incidence case.

	Thickness [mm]	Diameter [mm]	Porosity	Mass per unit area [kg/m^2]	Distance to next panel [m]
Panel 1	**0.800**	0.178	0.059	0.532	0.099
Panel 2	**0.800**	**0.100**	0.012	0.424	0.154
Panel 3	**0.800**	**0.100**	0.011	**0.800**	0.040
Panel 4	**0.800**	0.178	0.012	0.626	0.137
Panel 5	**0.800**	0.178	0.012	0.592	-

In Figure 6.7, it can be seen that the results of the maximum resistance set brings much higher peak transmission loss, but recall that the goal of the optimization is not only maximizing the transmission loss but also removing the valley points. From this point-of-view, the optimized set is very stable overall in the speech interference range.

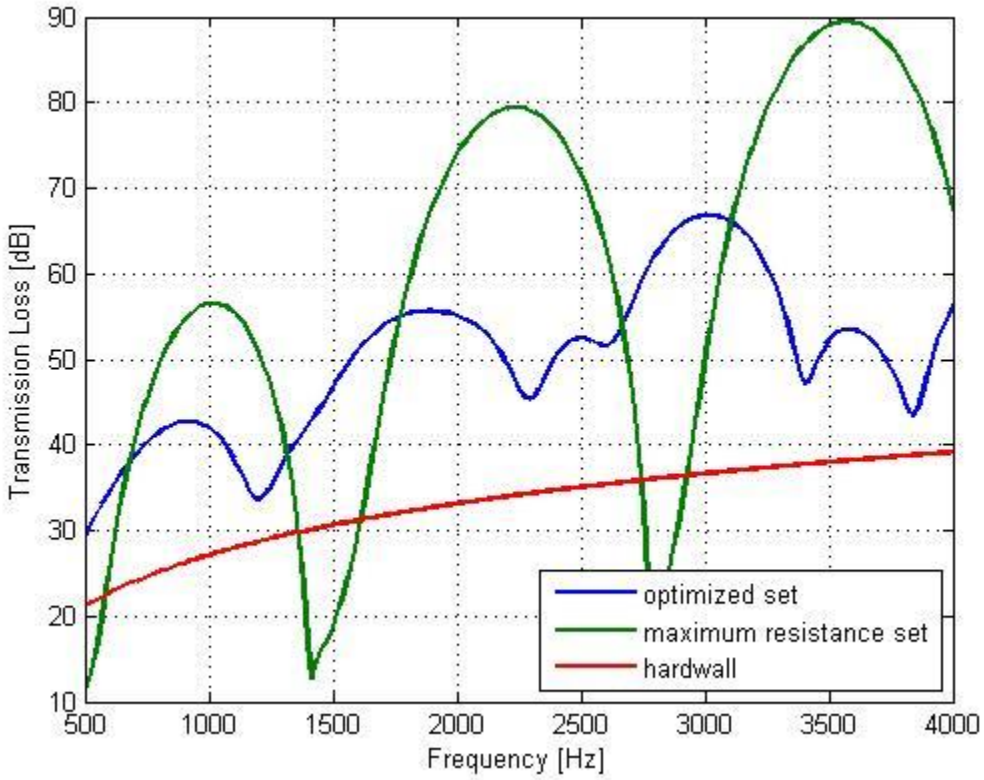

Figure 6.7. Comparison optimized set for normal incidence barrier case with maximum resistance set (5 panels).

6.3 Random Incidence

The random incidence case means that sound passes through the multi-layer MPP in random directions. As mentioned earlier, only the locally reacting case was considered, and the genetic algorithm method was used as the optimization method and $\sum 1/TL$ was used for the error function. Figure 6.8 is the result of the optimization as a function of the number of panels. Figure 6.8(a) shows the change of error with number of panels and Fig. 6.8(b) is a comparison of the optimization results by changing the number of panels. From Figure 6.8(a), 6 panels were chosen for the optimized barrier for the random incidence case, and Table 6.2 is the result of the optimization.

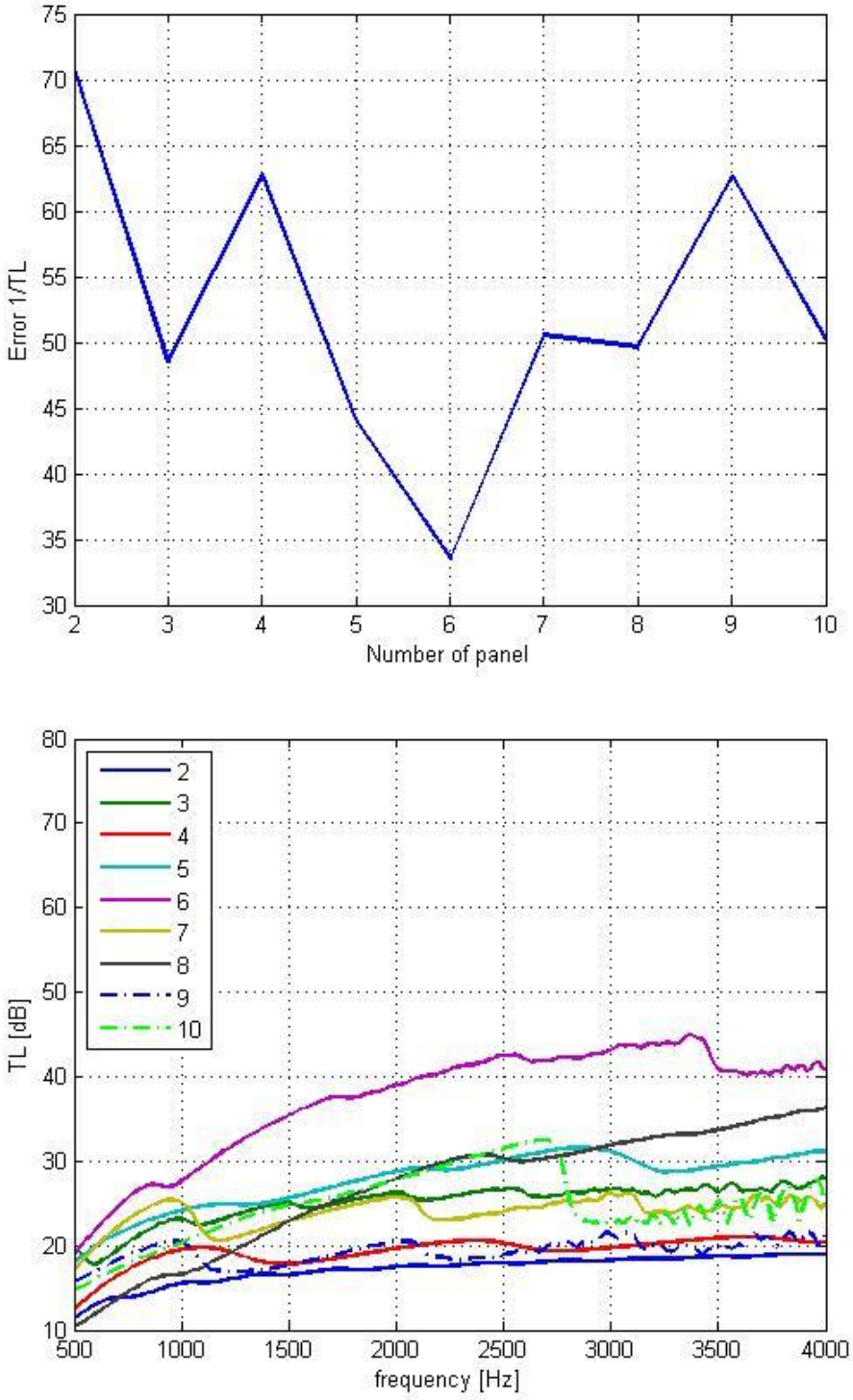

Figure 6.8. Optimization results by number of panels for random incidence barrier.

Table 6.2. Optimized set for a barrier in random incidence case.

	Thickness [mm]	**Diameter [mm]**	**Porosity**	**Mass per unit area [kg/m^2]**	**Distance to next panel [m]**
Panel 1	**0.800**	**0.300**	0.073	0.376	**0.200**
Panel 2	0.749	**0.100**	0.010	0.700	**0.200**
Panel 3	**0.800**	**0.100**	0.010	0.730	0.036
Panel 4	**0.800**	**0.300**	0.200	0.701	0.002
Panel 5	**0.800**	**0.300**	0.138	0.133	0.005
Panel 6	0.765	**0.100**	0.010	0.350	-

In Figure 6.9, it can be seen that as in the normal incidence case, the transmission loss of the maximum resistance set reaches a higher peak level in the overall range, but the transmission loss of the optimized set is much smoother and doesn't show resonance frequencies. This means that the optimized barrier displays no noise leakage at particular frequencies, so we can say that the optimization result is much improved compared with the maximum resistance set.

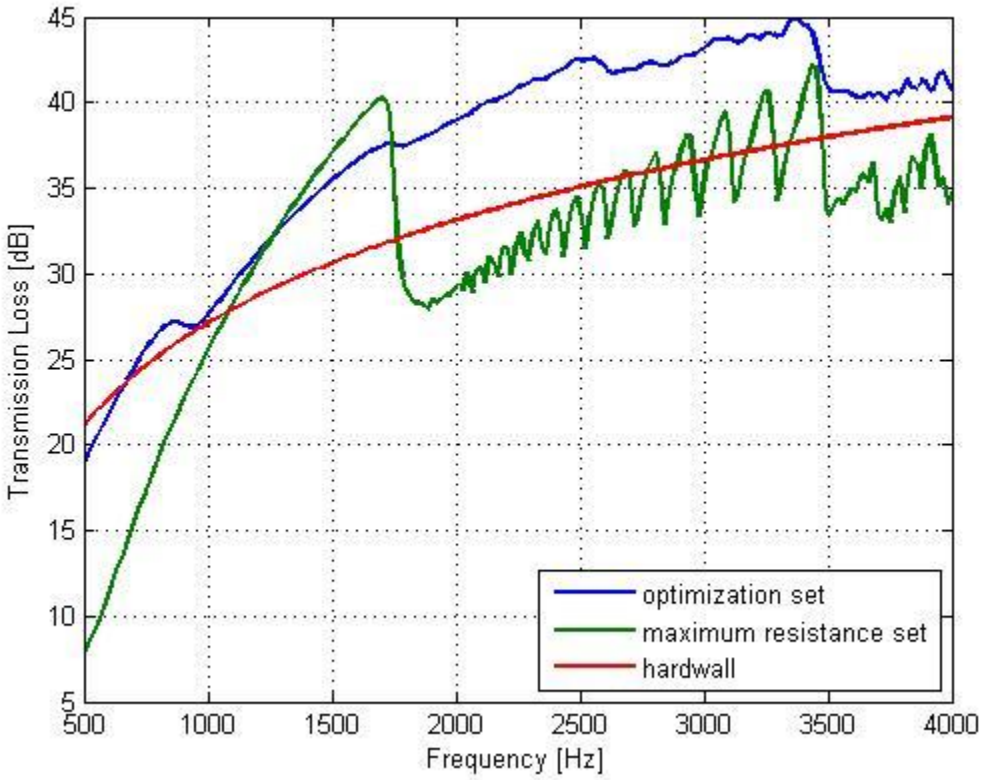

Figure 6.9. Comparison optimized set for random incidence barrier case with maximum resistance set (6 panels).

6.4 Summary

In this chapter, the transmission loss of multi-layers of microperforated panels was discussed. An appropriate combination of microperfoated panels can provide excellent performance for transmission loss and also can remove the valley points. This suggests that hard and heavy acoustic barrier can be replaced with a proper combination of a layered array of MPPs.

Here, only the local reaction case was considered, but if the analysis were also to consider the extended reaction case, which means there would be no need to separate

each panel with an “egg crate” lattice, an even lighter sound absorption material could be produced.

CHAPTER 7. PARTITION

In Chapters 5 and 6, optimization was performed for the dissipation coefficient and transmission loss. But for partitions in an office area or at the home, both the dissipation coefficient and transmission loss are important. In an indoor case, even when a noise source is in one area, the barrier should be designed to minimize reflected noise from the partition.

7.1 Optimization

The main purpose of a partition is to absorb sound and also to block noise from the noise source in a specific frequency range. So both the dissipation coefficient and transmission loss of system must be optimized. In this case, both directions were considered for dissipation coefficients and only one direction was considered for transmission loss, and the objective of the optimization was to maximize the dissipation coefficient and at the same time to minimize transmission loss, so the error function was chosen to be as $\sum 1 - \alpha_d + \beta T$, where T is transmission coefficient and β is impact factor. In this work, β was chosen as 0.8 to achieve a balance between transmission coefficient and absorbing coefficient, but to give a little bit more emphasis on blocking the noise from source. Two different cases, normal and random incidence case, were considered in this work.

7.2 Normal Incidence

The optimization for the normal incidence partition case was calculated by using the genetic algorithm, and Figure 7.1 shows the error by number of panels and Figure 7.2 shows that the dissipation coefficient and transmission loss by number of panels. Based on Figure 7.1, a 6 panels system is the best case at normal incidence, and the parameters of this system are listed in Table 7.1.

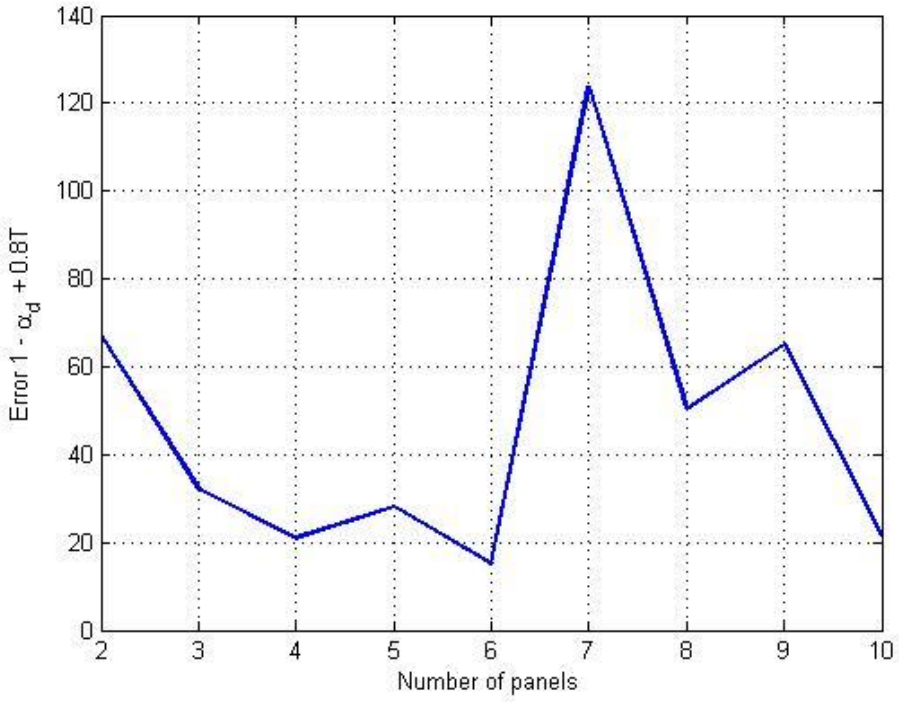

Figure 7.1. Error by number of panels for normal incidence partition.

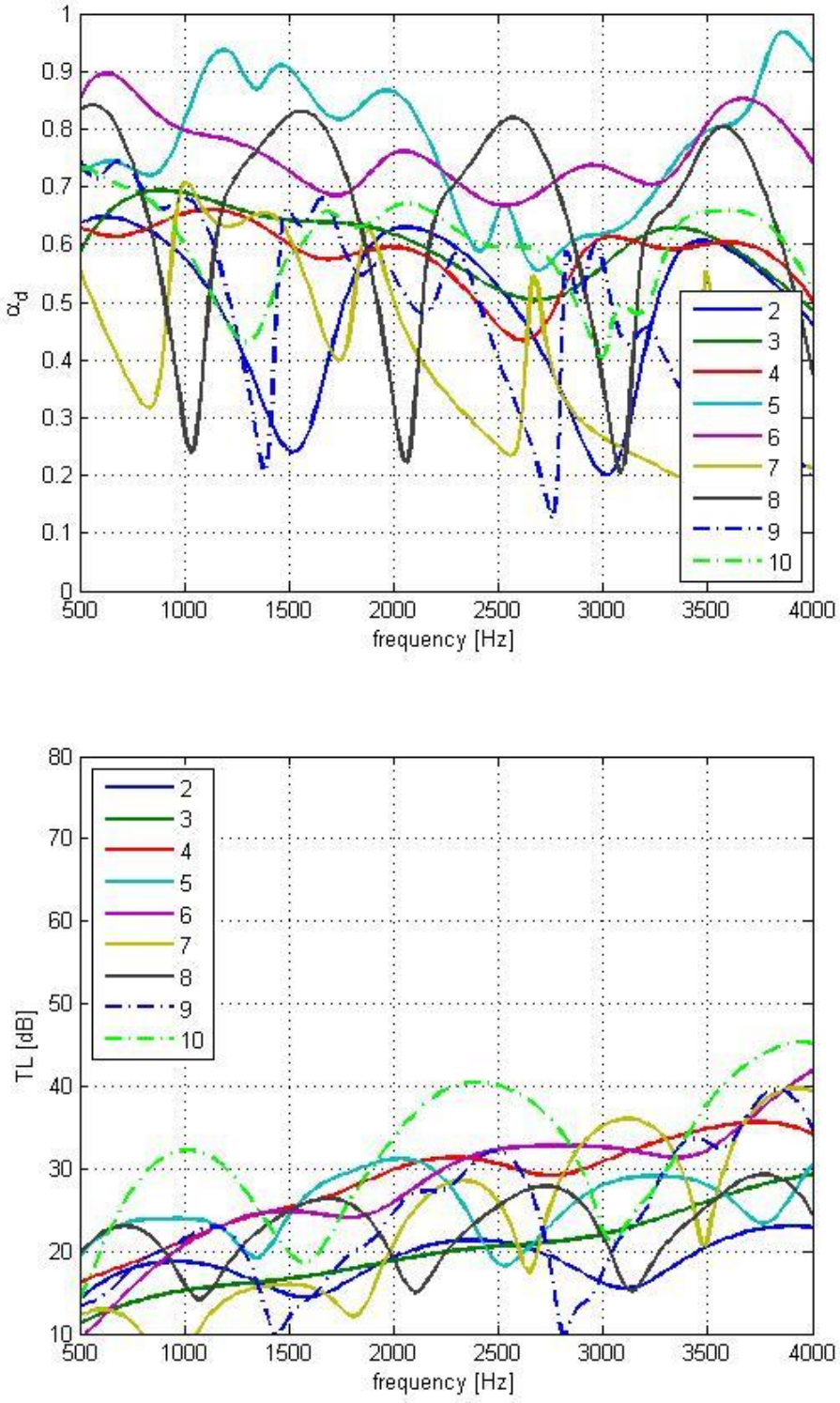

Figure 7.2. Optimization results by number of panels for normal incidence partition.

Table 7.1. Optimized set for a partition in normal incidence case.

	Thickness [mm]	Diameter [mm]	Porosity	Mass per unit area [kg/m^2]	Distance to next panel [m]
Panel 1	0.333	0.178	0.076	0.555	0.070
Panel 2	0.201	0.178	0.029	0.429	0.072
Panel 3	0.280	0.107	0.026	0.350	0.032
Panel 4	**0.800**	**0.100**	0.010	0.272	0.029
Panel 5	**0.800**	0.178	0.133	0.352	0.069
Panel 6	**0.800**	**0.100**	0.039	0.201	-

For comparison, the optimized results for a functional absorber (Chapter 5) and a barrier (Chapter 6) were used. Figures 7.3 and 7.4 show the comparison between the dissipation coefficient and the transmission loss of an optimized functional absorber and of an optimized partition, and between the optimized barrier and the optimized partition. As shown as Figure 7.3, the dissipation coefficient of the functional absorber provides better performance than that of the partition, but the transmission loss of the partition is higher than that of the functional absorber in the whole frequency range. In Figure 7.4, the transmission loss of the barrier can be seen to be much better than that of the partition, but the dissipation coefficient of the partition is much higher than that of a barrier. Note that the goal of the optimization in this chapter was to achieve a balance between the dissipation coefficient and the transmission loss. So the partition case does not give the best performance for either the dissipation coefficient or the transmission loss, but it does offer a balance between the two acoustic requirements.

.

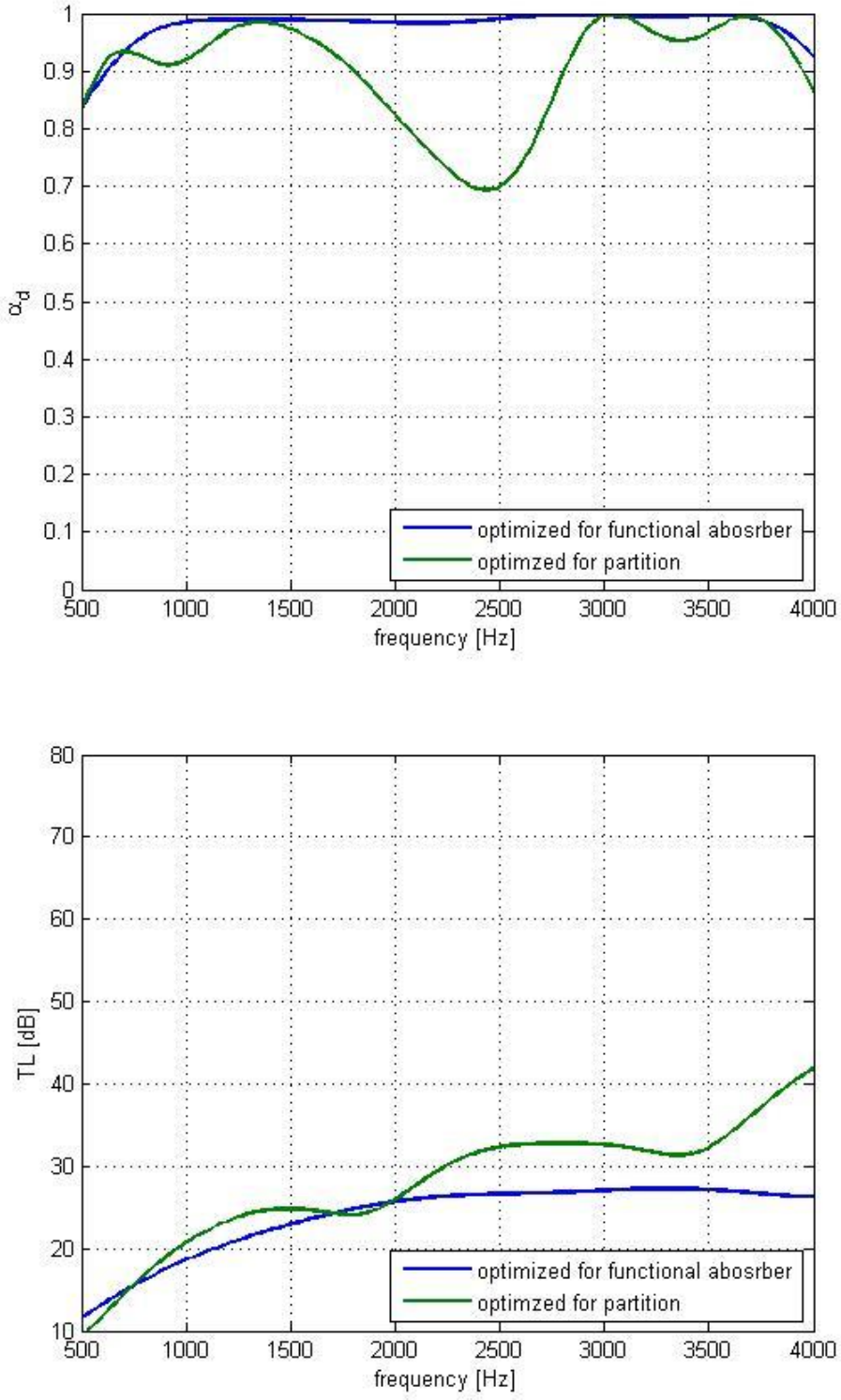

Figure 7.3. Dissipation coefficient and transmission loss of functional absorber and partition for normal incidence.

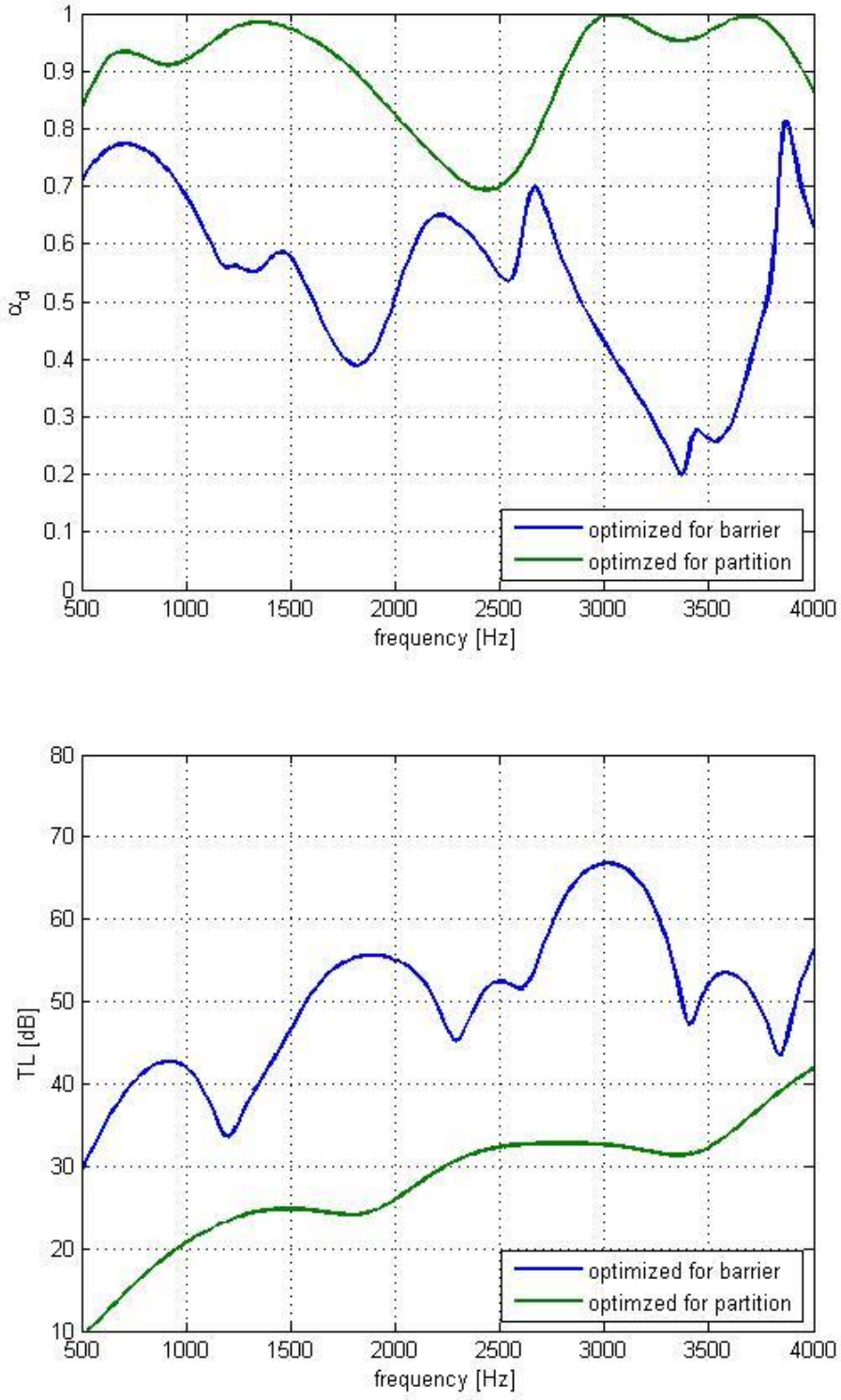

Figure 7.4. Dissipation coefficient and transmission loss of barrier and partition for normal incidence.

7.3 Random Incidence

As for the normal incidence case, the optimization for random incidence was calculated by using the genetic algorithm. Figure 7.5 shows the error by number of panels and Figure 7.6 shows the dissipation coefficient and the transmission loss by the number of panels. An 8 panels system was chosen for a partition in the random incidence case based on Figure 7.5, and the parameters of this system are listed in Table 7.2.

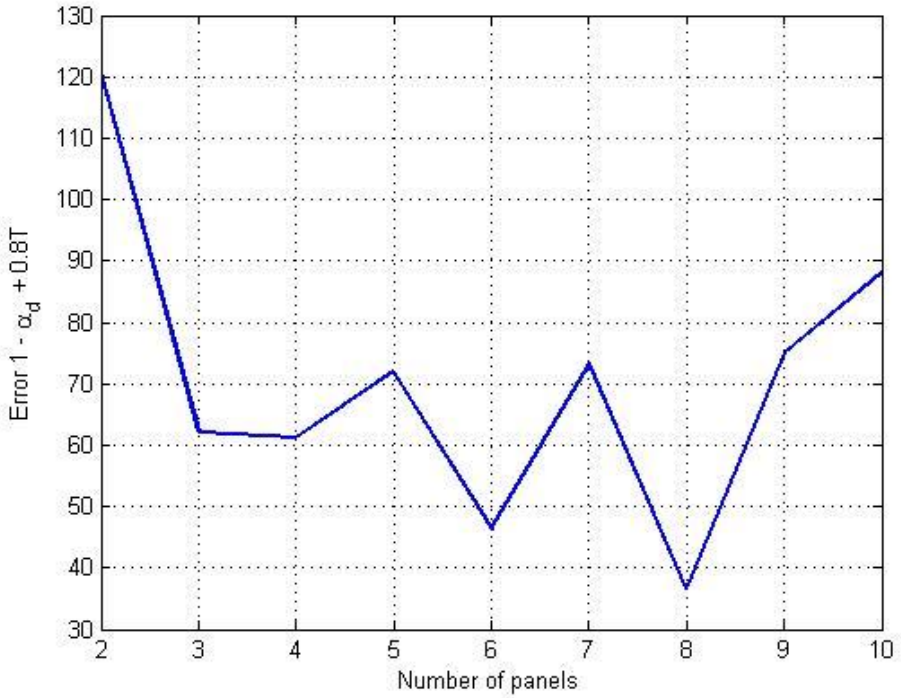

Figure 7.5. Error by number of panels for random incidence partition.

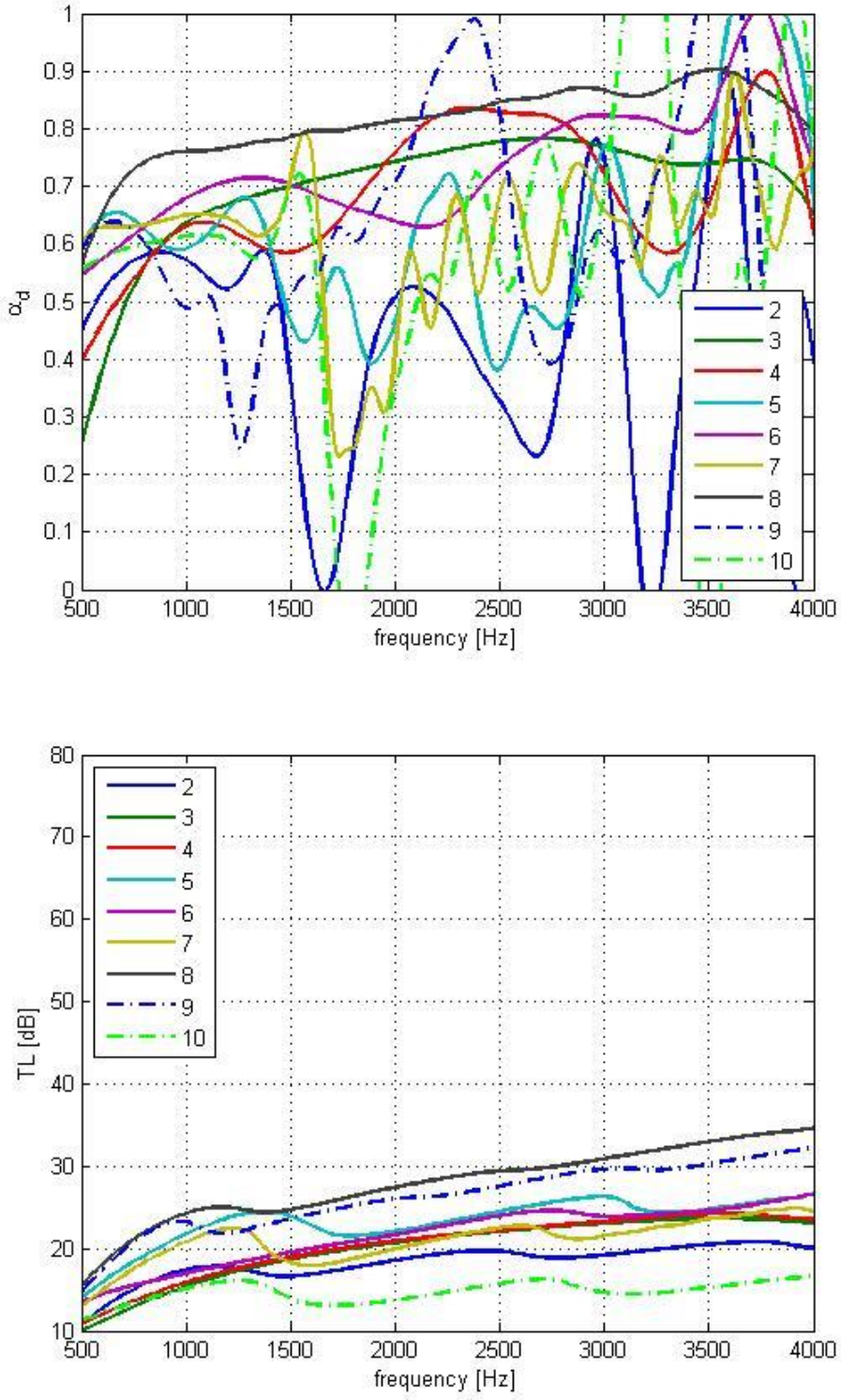

Figure 7.6. Optimization results by number of panels for random incidence partition.

Table 7.2. Optimized set for a partition in random incidence case.

	Thickness [mm]	Diameter [mm]	Porosity	Mass per unit area [kg/m^2]	Distance to next panel [m]
Panel 1	**0.800**	**0.300**	0.113	**0.100**	0.030
Panel 2	**0.800**	**0.300**	0.105	0.140	0.023
Panel 3	**0.800**	**0.300**	0.183	0.382	0.017
Panel 4	**0.800**	0.176	0.042	**0.100**	0.024
Panel 5	0.780	0.300	0.076	0.112	0.004
Panel 6	0.234	0.193	0.015	0.631	0.031
Panel 7	**0.800**	**0.100**	0.035	0.644	0.136
Panel 8	**0.800**	**0.100**	0.010	0.618	-

As in the normal incidence case, the optimized results for a functional absorber (Chapter 5) and a barrier (Chapter 6) were used for a comparison. Figure 7.7 is the comparison of the acoustic performance between a functional absorber and the partition, and Figure 7.8 shows a comparison of the acoustic performance between a barrier and a partition. As seen as Figure 7.7, the dissipation coefficient of a functional absorber is better than that of the partition but the transmission loss of the partition is higher than that of the functional absorber in the whole frequency range. In Figure 7.8, the transmission loss of the barrier is much better than that of a partition, but the dissipation coefficient of the partition is much higher than that of the barrier, especially in the high frequency range. So the partition case does not provide the best performance for the dissipation coefficient or for the transmission loss, but it is well balanced in terms of the two acoustic performance metrics.

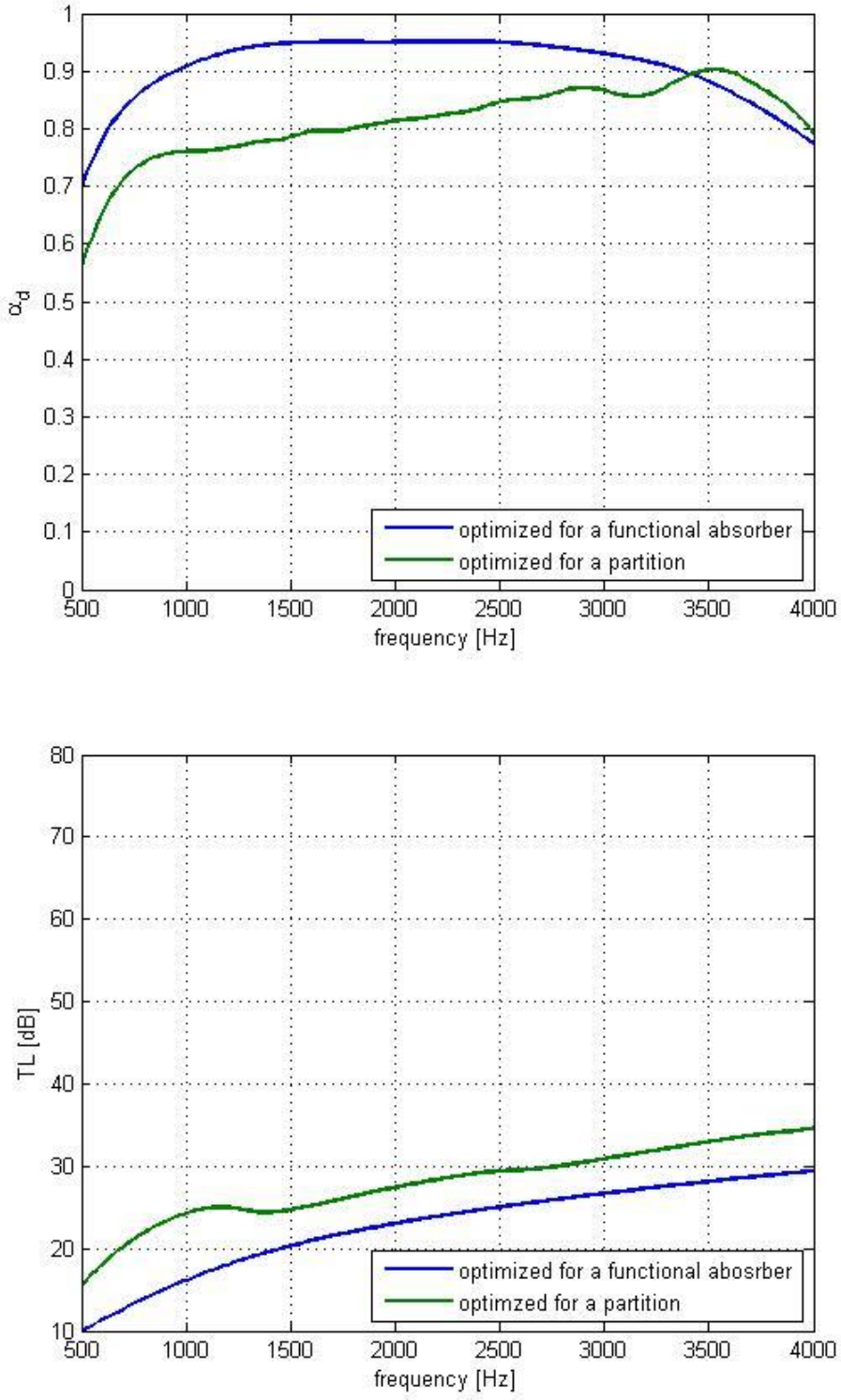

Figure 7.7. Dissipation coefficient and transmission loss of functional absorber and partition for random incidence.

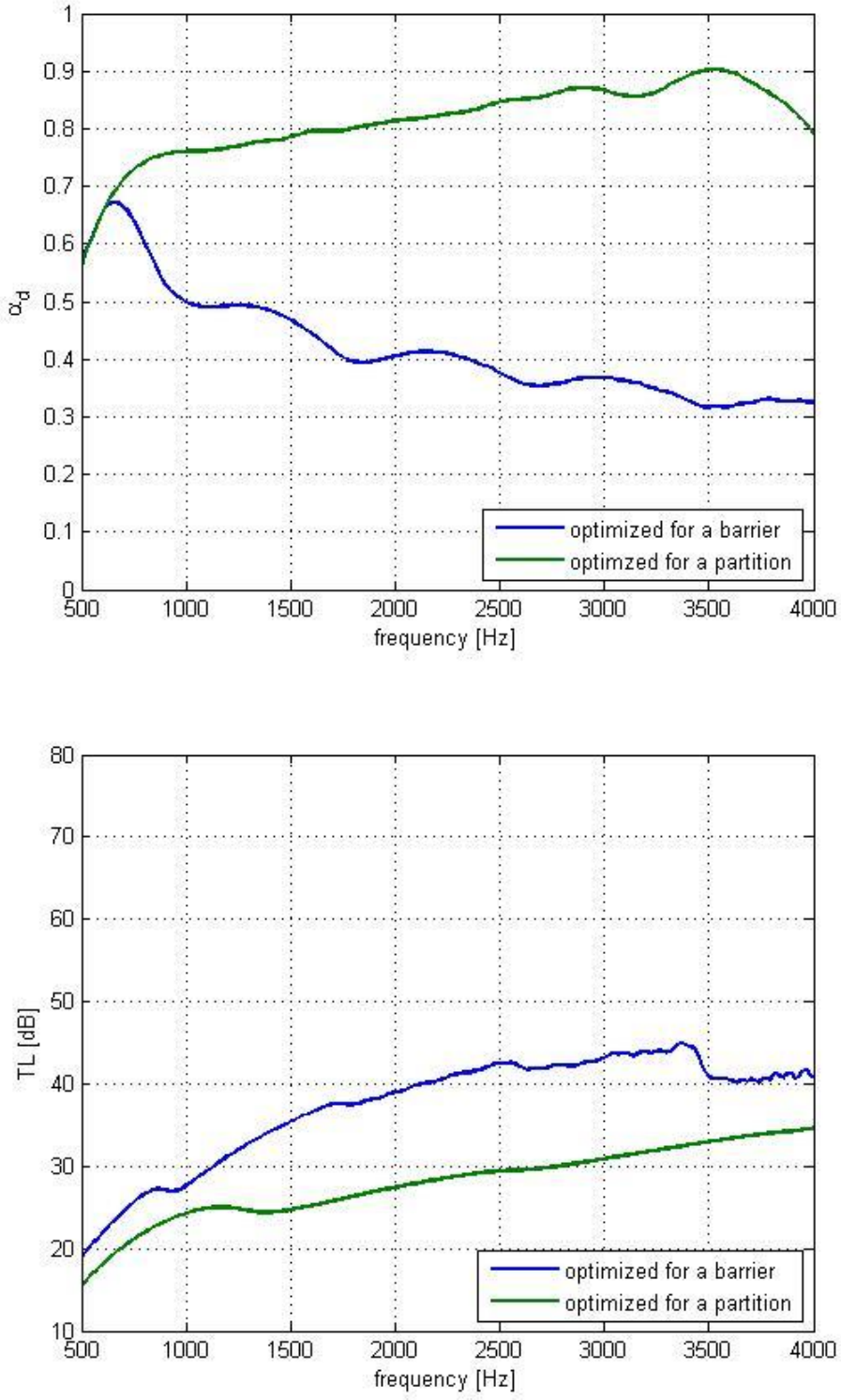

Figure 7.8. Dissipation coefficient and transmission loss of barrier and partition for random incidence.

7.4 Summary

In this chapter, to optimize the dissipation coefficient and the transmission loss simultaneously, the error function $\sum 1 - \alpha_d + 0.8T$ was used. It provided a good combinations of microperforated panels to fit both function. Compared with a functional absorber case, or a barrier case, the partition does not provide the best performance for either metric, but it is well balanced in terms of the dissipation coefficient and the transmission loss.

Here, $\sum 1 - \alpha_d + \beta T$, when $\beta = 0.8$ was chosen by trial and error for the error function in the optimization calculation, but if the system has a specific purpose, then the constant modifying β can be changed for fitting that objective.

CHAPTER 8. OPTIMIZATION WITH SINGLE PANEL TYPE

Note that the design of an *N* multiple-layer MPP system depends on 5*N*-1 parameters, and so a general optimization becomes difficult in realistic cases when as many as ten layers might be used. If we can assume that the properties of each layers are the same, the number of parameter reduces to *N*+3 and calculation cost will be significantly reduced, especially when the system has many layers. If the acoustic performance of multi-layers microperforated panels with the same panel is similar to the case when all the panels are different, then it makes finding the optimal set of parameters easier. In this chapter, the same constraints are applied as before, and only the random incidence case was considered.

8.1 Functional Absorber

As in Chapter 5, the dissipation coefficient of the system is focused on as the quantity to optimize. Both directions of dissipation coefficients were considered, and the error function was chosen to be $\sum 1 - \alpha_d$, and genetic algorithm was used to perform the optimization.

Figure 8.1 shows that error by number of panels and dissipation coefficient of the optimized system versus the number of panels. Based on Figure 8.1, a 10 panels system

was the best performance for the functional absorber and the optimization result is given in Table 8.1.

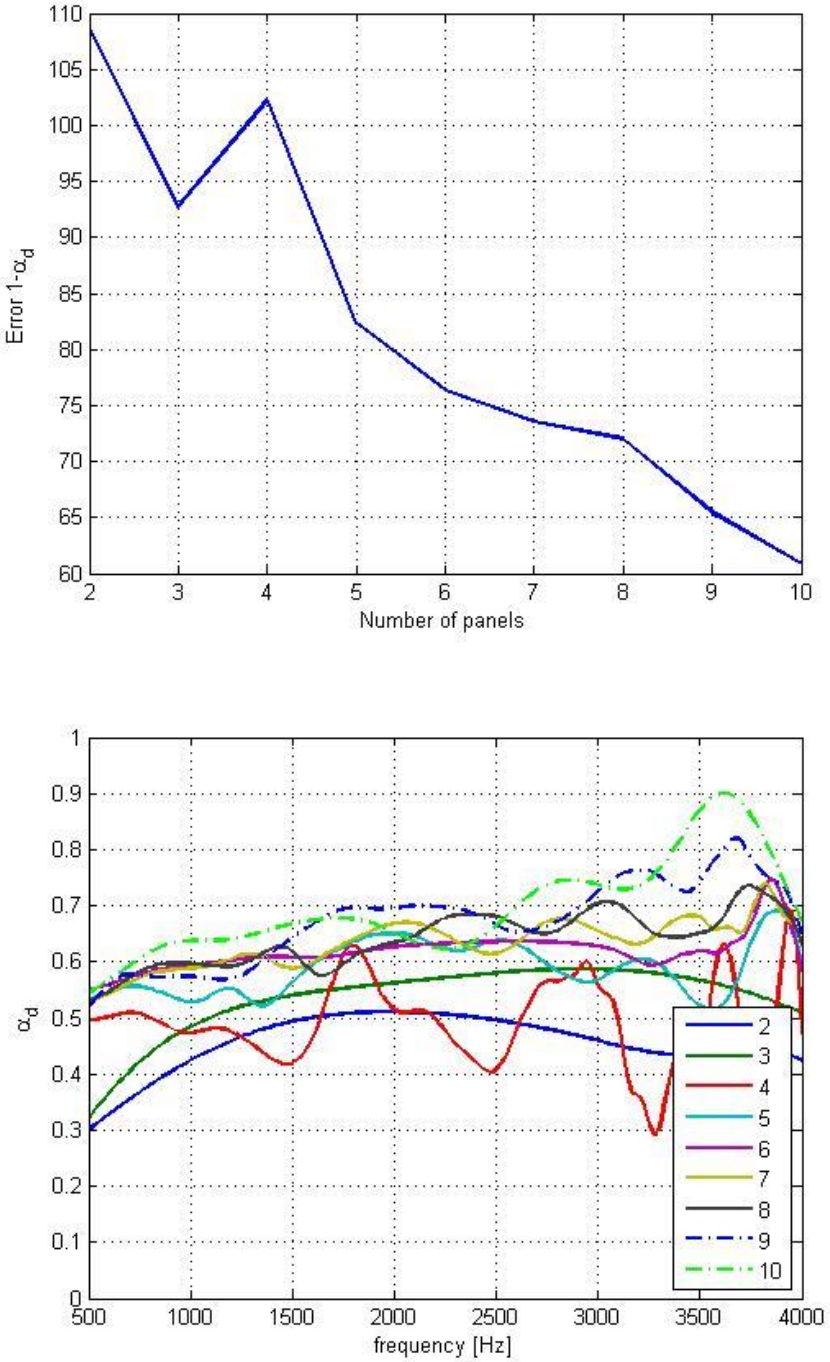

Figure 8.1. Optimization results by number of panels for functional absorber with same panel.

Table 8.1. Optimized set for a functional absorber with same panels in random incidence.

	Thickness [mm]	Diameter [mm]	Porosity	Mass per unit area [kg/m^2]	Distance to next panel [m]
Panel 1	0.737	0.239	0.049	0.299	0.026
Panel 2	0.737	0.239	0.049	0.299	0.038
Panel 3	0.737	0.239	0.049	0.299	0.027
Panel 4	0.737	0.239	0.049	0.299	0.054
Panel 5	0.737	0.239	0.049	0.299	0.001
Panel 6	0.737	0.239	0.049	0.299	0.054
Panel 7	0.737	0.239	0.049	0.299	0.026
Panel 8	0.737	0.239	0.049	0.299	0.039
Panel 9	0.737	0.239	0.049	0.299	0.026
Panel 10	0.737	0.239	0.049	0.299	-

Figure 8.2 shows the dissipation coefficient of a functional absorber having all different microperforated panels and with the same microperforated panels. The same panel system has a much lower calculation cost than the different panel system, but the result of the optimized set for the different panel system provides much better performance.

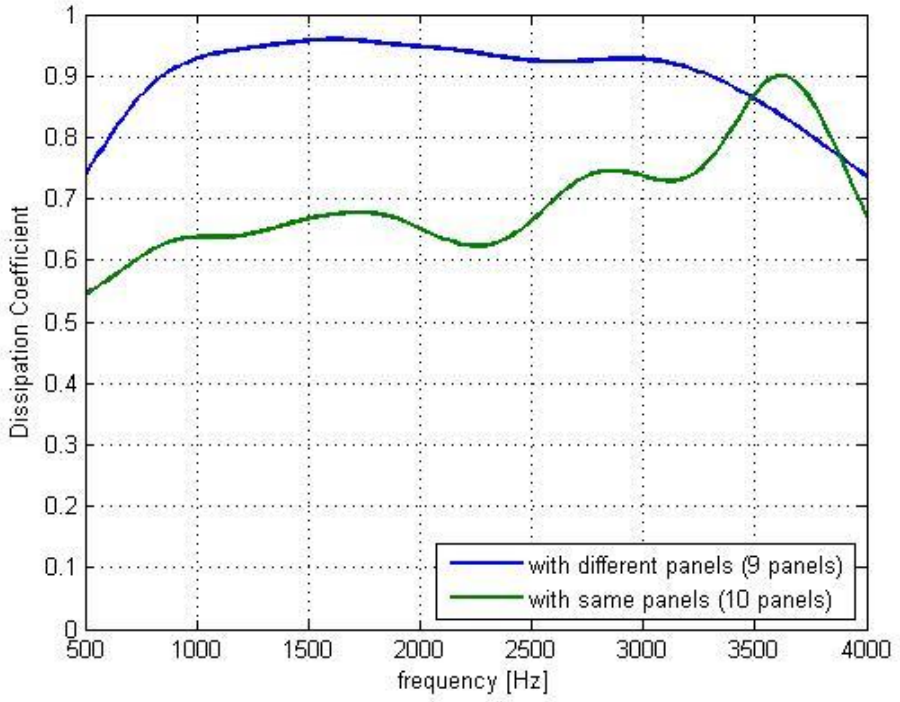

Figure 8.2. Different panel system vs same panel system (dissipation coefficient).

8.2 Barrier

The purpose of a barrier is to maximize the transmission loss, and also to eliminate resonances in the frequency range of interest as mentioned before. To satisfy these two conditions, the error function was set as $\sum 1/TL$, and the genetic algorithm was used for the optimization.

Figure 8.3 shows the error by number of panels and transmission loss of optimized system with same panel. Based on Figure 8.3, a 7 panels system was chosen for the best set for the barrier and the optimization result is given in Table 8.2.

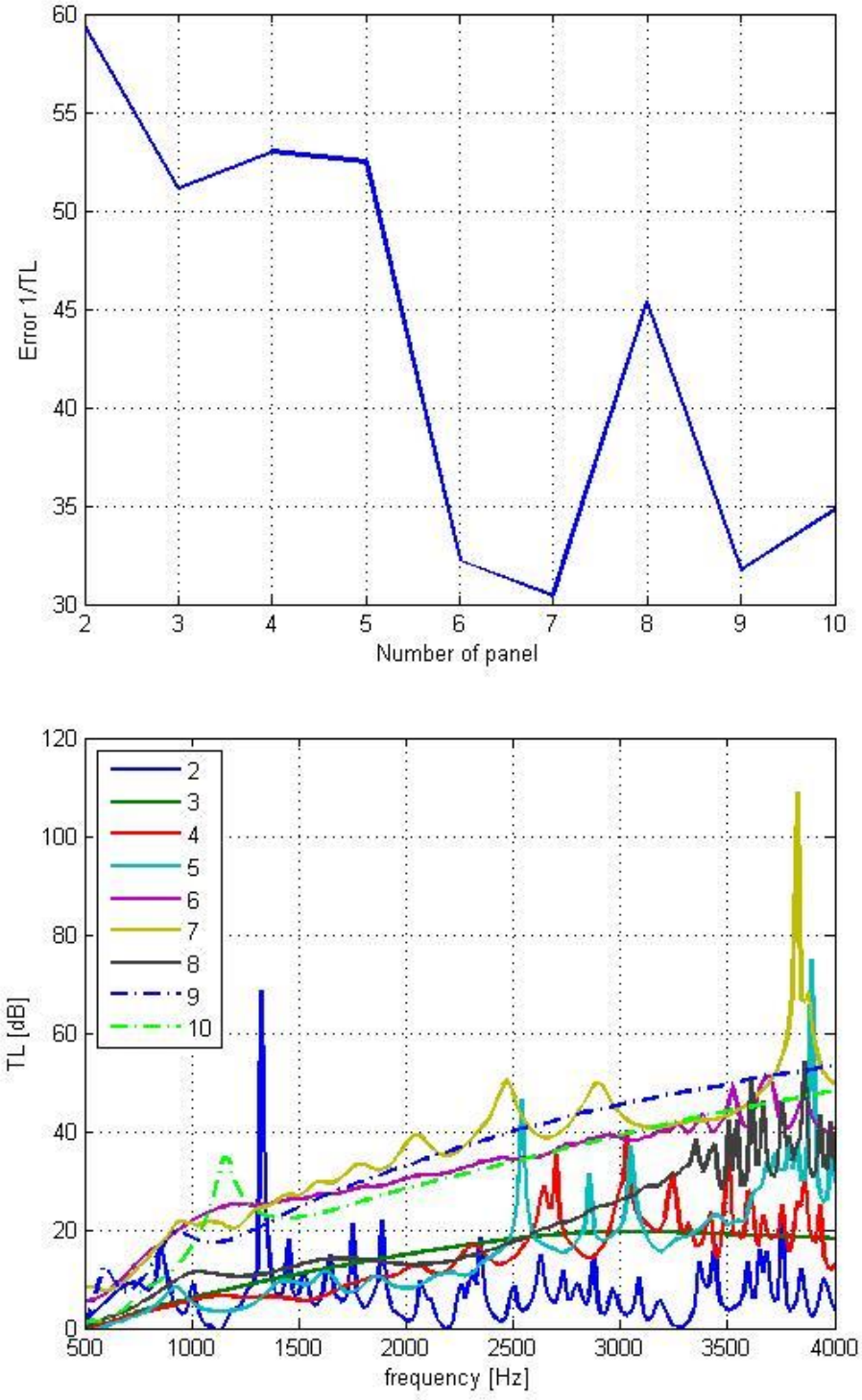

Figure 8.3. Optimization results by number of panels for barrier with same panel.

Table 8.2. Optimized set for a barrier with same panels in random incidence.

	Thickness [mm]	Diameter [mm]	Porosity	Mass per unit area [kg/m^2]	Distance to next panel [m]
Panel 1	0.773	0.101	**0.01**	0.429	0.001
Panel 2	0.773	0.101	**0.01**	0.429	0.017
Panel 3	0.773	0.101	**0.01**	0.429	0.017
Panel 4	0.773	0.101	**0.01**	0.429	0.200
Panel 5	0.773	0.101	**0.01**	0.429	0.048
Panel 6	0.773	0.101	**0.01**	0.429	0.191
Panel 7	0.773	0.101	**0.01**	0.429	

Figure 8.4 shows the transmission loss of a barrier with different microperforated panels and with the same microperforated panels. The same panel system seems to provide better performance in specific frequencies (over 2500 Hz), but due to the use of the same panel, resonances appear which makes the transmission loss fluctuate, and the transmission loss is too low in low frequency range. If the purpose is to provide consistent performance through the frequency range of interest, then the optimized set of the same panels system does not fit the purpose.

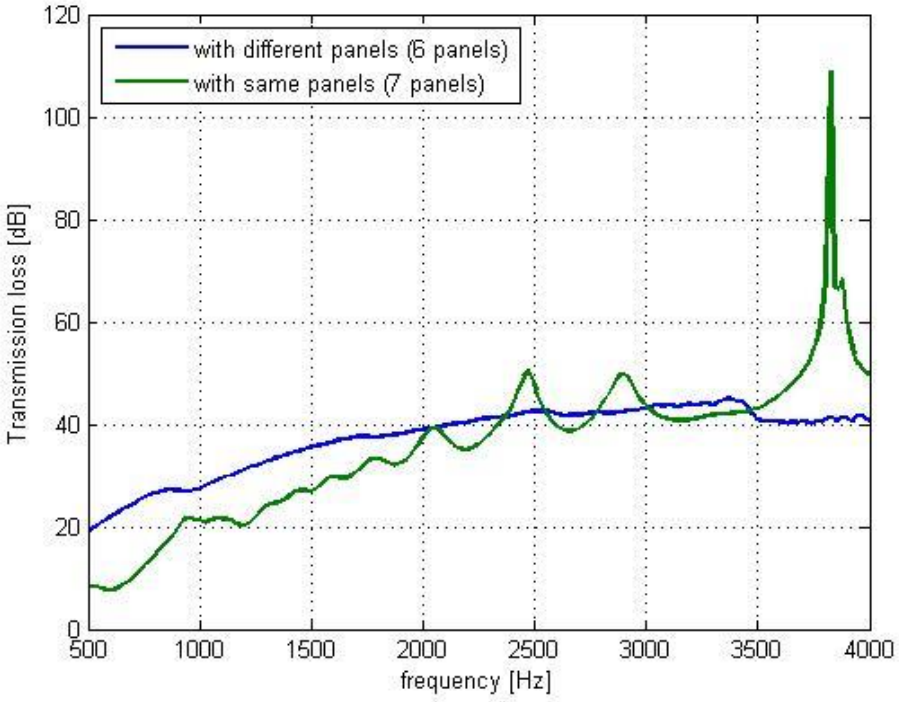

Figure 8.4. Different panel system vs same panel system (transmission loss).

8.3 Summary

In this chapter, to reduce the calculation cost lower, the optimization of multi-layers systems with the same panel elements was considered. This model can provide acceptable results in a shorter calculation time, but there is a fluctuation in the transmission loss, because of resonances due to the use of the same panels. To avoid resonance, combinations of two or three types of microperforated panel can be one of solution but there are still limitation to remove valley point in speech interference range. If you want to obtain a system with the consist performance in the frequency range of interest, then a multi-layer system with different panels is the answer.

.

CHAPTER 9. OPTIMAL DESIGN OF MULTI-LAYER MICROPERFORATED PANELS FOR CYLINDRICAL DUCT LINER

9.1 Analytic Solution

To calculate the performance of a duct liner for a cylindrical duct, a transfer matrix in cylindrical coordinates is needed. Figure 9.1 is the geometry of a cylindrical duct liner.

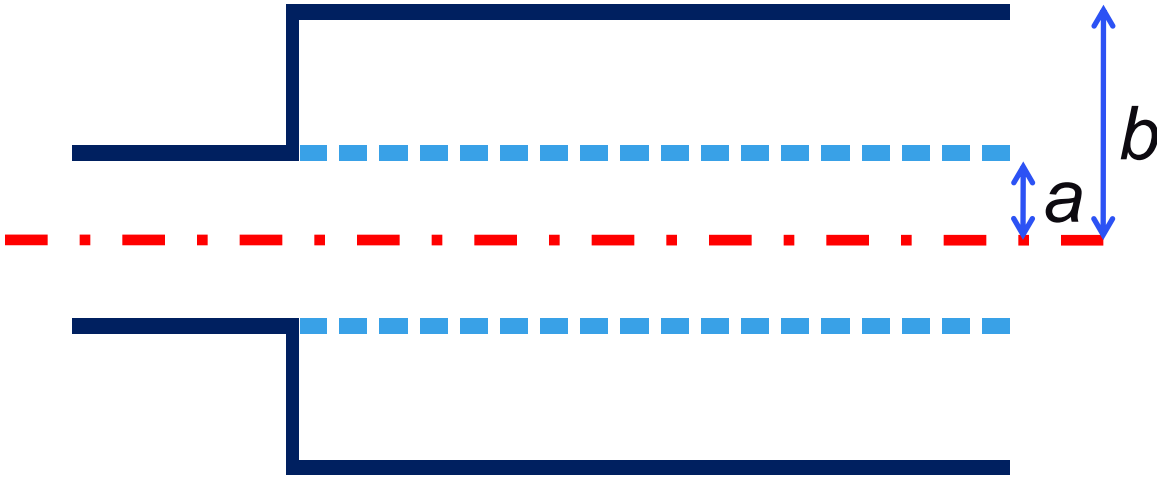

Figure 9.1. The geometry of the single cylindrical duct liner.

To find the surface impedance at the liner, start from the Helmholtz equation.

$$(\nabla^2 + k^2)\vec{P}(r, \theta, z) = 0. \tag{9.1}$$

It is assumed that the pressure is symmetric in the θ direction; the pressure and velocity of air can then be expressed as,

$$\vec{P}(\omega, r, z) = [AH_0^{(1)}(k_r r) + BH_0^{(2)}(k_r r)]e^{j(k_z z - \omega t)} \quad (9.2)$$

$$\vec{v}(\omega, r, z) = \frac{j}{\rho c}\frac{k_r}{k}[AH_1^{(1)}(k_r r) + BH_1^{(2)}(k_r r)]e^{j(k_z z - \omega t)} \quad (9.3)$$

$$k^2 = k_r^2 + k_z^2 \quad (9.4)$$

Here, P is sound pressure, v is the particle velocity, k_r is the wave number in the r-direction, k_z is wave number in the z-direction, ρ is the density of air, c is the sound speed, A and B are constants, $H_0^{(1)}$is the zero order Hankel function of the first kind, $H_0^{(2)}$ is the zero order Hankel function of the second kind, $H_1^{(1)}$is the first order Hankel function of the first kind, and $H_1^{(2)}$ is the first order Hankel function of the second kind.

In Figure 9.1, the pressure and velocity at the liner and the wall can be expressed as,

$$\overrightarrow{p_a} = [AH_0^{(1)}(k_r a) + BH_0^{(2)}(k_r a)]e^{j(k_z z - \omega t)} \quad (9.5)$$

$$\overrightarrow{v_a} = \frac{j}{\rho c}\frac{k_r}{k}[AH_1^{(1)}(k_r a) + BH_1^{(2)}(k_r a)]e^{j(k_z z - \omega t)} \quad (9.6)$$

$$\overrightarrow{p_b} = [AH_0^{(1)}(k_r b) + BH_0^{(2)}(k_r b)]e^{j(k_z z - \omega t)} \quad (9.7)$$

$$\overrightarrow{v_b} = \frac{j}{\rho c}\frac{k_r}{k}[AH_1^{(1)}(k_r b) + BH_1^{(2)}(k_r b)]e^{j(k_z z - \omega t)} \quad (9.8)$$

where P_a is the pressure at the liner, v_a is the particle velocity at the liner, P_b is the pressure at the wall, and v_b is the particle velocity at the wall. To calculate impedance of the annular air space, the transfer matrix method was used; i.e.,

$$\begin{bmatrix} p_a \\ v_a \end{bmatrix} = [D]\begin{bmatrix} A \\ B \end{bmatrix} \tag{9.9}$$

$$\begin{bmatrix} p_b \\ v_b \end{bmatrix} = [E]\begin{bmatrix} A \\ B \end{bmatrix} = [E][D]^{-1}[D]\begin{bmatrix} A \\ B \end{bmatrix} = [E][D]^{-1}\begin{bmatrix} p_a \\ v_a \end{bmatrix} \tag{9.10}$$

$$[T] = [E][D]^{-1} = \begin{bmatrix} T_{11} & T_{12} \\ T_{21} & T_{22} \end{bmatrix} \tag{9.11}$$

where T is the transfer matrix of the air space between at a and at b. Based on Eqs. (9.5) to (9.11), the transfer matrix can be calculated as

$$T_{11} = -j\frac{\pi}{4}k_r a\,[H_0^{(1)}(k_r b)H_1^{(2)}(k_r a) - H_0^{(2)}(k_r b)H_1^{(1)}(k_r a)] \tag{9.12.a}$$

$$T_{12} = \frac{\pi}{4}\rho c k a\,[H_0^{(1)}(k_r b)H_0^{(2)}(k_r a) - H_0^{(2)}(k_r b)H_0^{(1)}(k_r a)] \tag{9.12.b}$$

$$T_{21} = \frac{\pi}{4}\frac{1}{\rho c}\frac{k_r}{k}a\,[H_1^{(1)}(k_r b)H_1^{(2)}(k_r a) - H_1^{(2)}(k_r b)H_1^{(1)}(k_r a)] \tag{9.12.c}$$

$$T_{22} = -j\frac{\pi}{4}k_r a\,[H_1^{(2)}(k_r b)H_0^{(1)}(k_r a) - H_1^{(1)}(k_r b)H_0^{(2)}(k_r a)]. \tag{9.12.d}$$

From Eq. (9.12), the acoustic impedance looking into the liner can be expressed as

$$Z_{air} = \frac{T_{11}}{T_{21}} = -j\rho c k\left[\frac{H_0^{(1)}(k_r b)H_1^{(2)}(k_r a) - H_0^{(2)}(k_r b)H_1^{(1)}(k_r a)}{H_1^{(1)}(k_r b)H_1^{(2)}(k_r a) - H_1^{(2)}(k_r b)H_1^{(1)}(k_r a)}\right] \tag{9.13}$$

$$z_n = \frac{Z_{air} + Z_{MPP}}{\rho c} \tag{9.14}$$

where Z_{air} is the impedance of the air space, Z_{MPP} is the transfer impedance of the microperforated panel, and z_n is the surface impedance at $r = a$. Recall that the impedance of microperforated panel can be expressed as:

$$Z_{mpp} = \frac{R\sigma(1-\sigma)(j\omega m - j\omega\rho(t+2\delta)) + j\omega\rho(t+2\delta)\{j\omega m(1-\sigma)+R\sigma\}}{\sigma(1-\sigma)(R+j\omega m)+(1-\sigma)^2\rho(t+2\delta)j\omega+\sigma^2 R} \quad . \tag{4.16}$$

The boundary condition at $r = a$, then becomes

$$\frac{jka}{z_n} = m - \frac{k_r a J_{m-1}(k_r a)}{J_m(k_r a)} \tag{9.15}$$

where m is the mode number and J is the Bessel function. Equation (9.15) can be solved by the secant method and finally the transmission loss can be expressed as

$$k_z = \sqrt{k^2 - k_r^2} = \beta - j\alpha \tag{9.16}$$

$$TL = -20\log\left(\frac{1}{e^{\alpha}}\right) \quad \text{[dB/m]}. \tag{9.17}$$

9.2 Optimization

Here, only the local reaction case was considered and symmetry in the θ direction was assumed. The limits on the panel parameters were: diameter of inlet hole is 0.0001 to 0.0004 m; thickness of panel is 0.0001 to 0.001 m; porosity is 0.001to 0.1; and mass per unit area is 0.3 to 1 kg/m^2. The genetic algorithm was used for the optimization, and the

error function was set as $1/TL$ in the frequency range 500 to 5000 Hz, and Figure 9.2. shows the geometry of the duct used in this work.

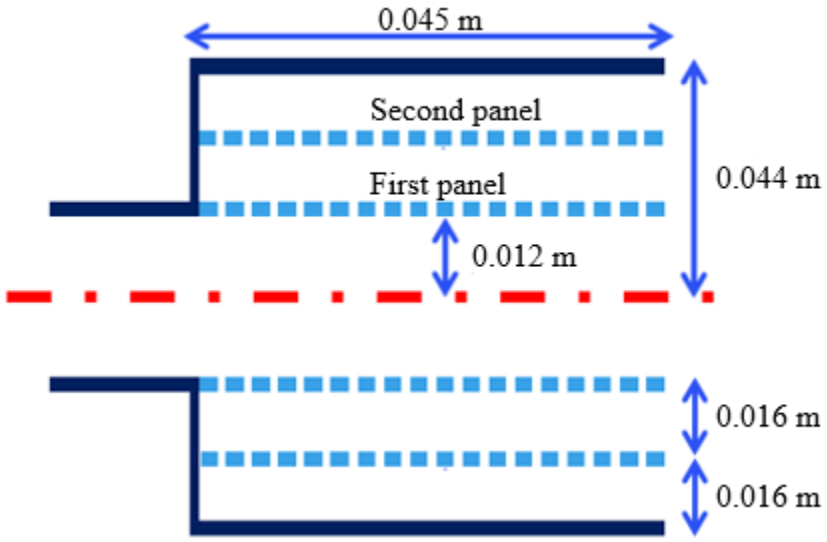

Figure 9.2. The geometry of cylindrical duct liner.

Before the optimization, to illustrate the main trends, a double panel liner was used. For the double panel case, the same distance was used between the first and the second panel and between the second panel and the wall, which was 0.016 m. And the first panel was fixed as t = 0.4064 mm, d = 0.2032 mm, σ =0.02, and m = 0.5 kg/m^2, and changes were made to the second panel parameters. The results are shown in Figure 9.3 to 9.6. As shown in the figures, if the panel is thin enough or porosity is high enough or the hole diameter is large enough, then the transmission loss is increased in the overall speech interference range. Note that all parameters work in the opposite way in the low frequency range (below 2000 Hz) but at around 3000 Hz, which is a valley point here, the parameters impact is the same as in the overall speech interference range. There is no big

impact on the transmission loss of the system by changing the mass per unit area of the second liner.

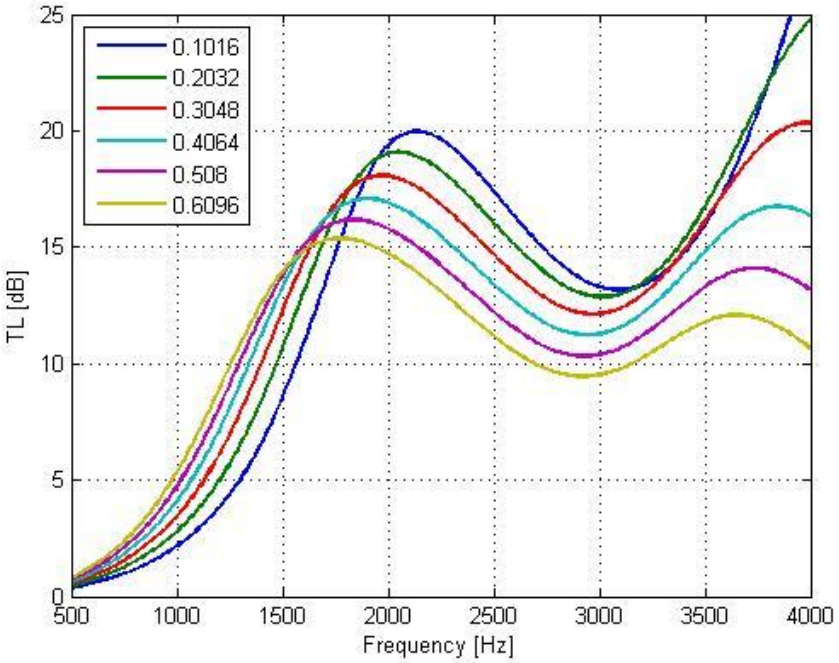

Figure 9.3. Transmission loss of 0.045 m length changing by thickness of the second panel.

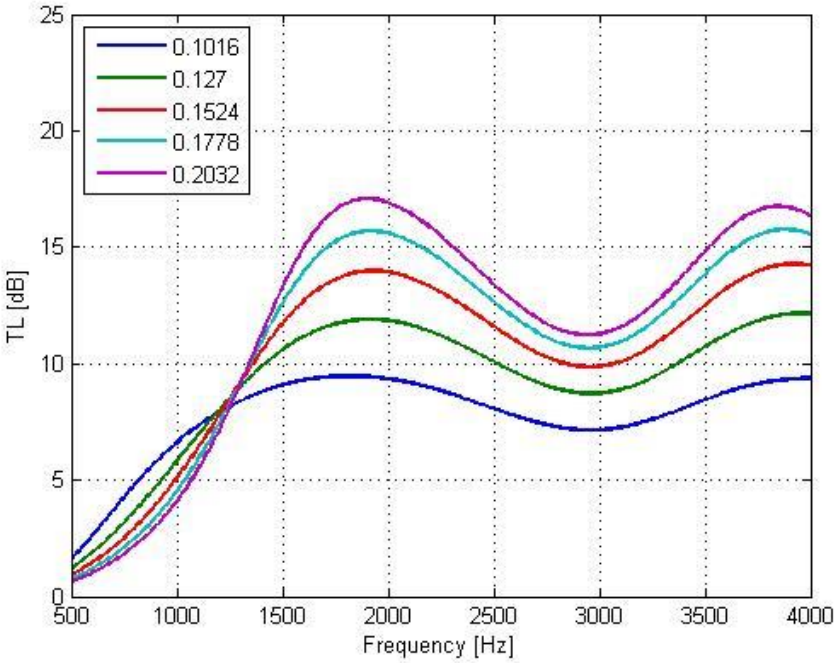

Figure 9.4. Transmission loss of 0.045 m length changing by porosity of the second panel.

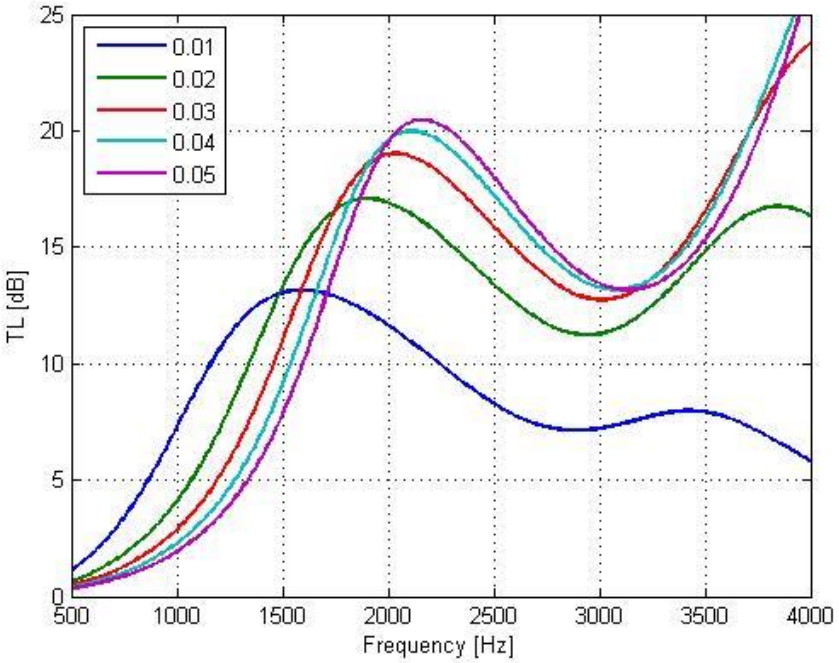

Figure 9.5. Transmission loss of 0.045 m length changing by hole diameter of the second panel.

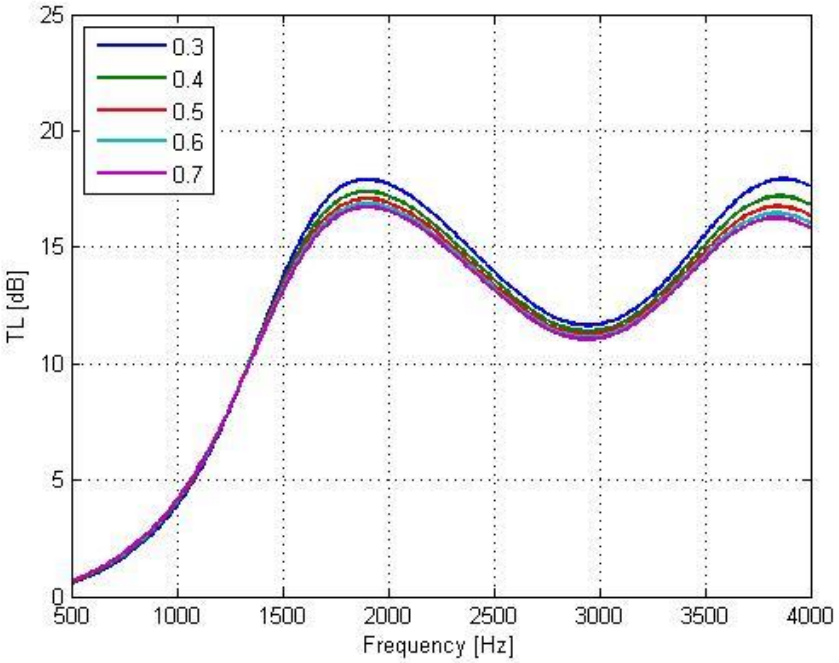

Figure 9.6. Transmission loss of 0.045 m length changing by mass per unit area of the second panel.

9.3 Result

The optimization was performed for single, double and triple microperforated panels. As mentioned earlier, the genetic algorithm was used to perform the optimization, and the variables were thickness, hole diameter, porosity, and mass per unit area of each panel, and the distance between the panels if there is more than 1 panel. Figure 9.7 shows the optimization result of single, double, and triple microperforated panel liners in the cylindrical duct. The objective in this research is maximizing transmission loss in the 500 to 5000 Hz range. The muffler without any liner has the best performance in the overall range. However, there is a resonance frequency at about 3800 Hz, and this resonance frequency is related to the length of the muffler. So the result of the optimization with duct liner shows the possibility to cover a wide frequency range with a short muffler length. The multiple duct liner reduces the maximum transmission loss in specific frequency ranges, but it can shift the resonance frequency to frequencies out of the range of interest.

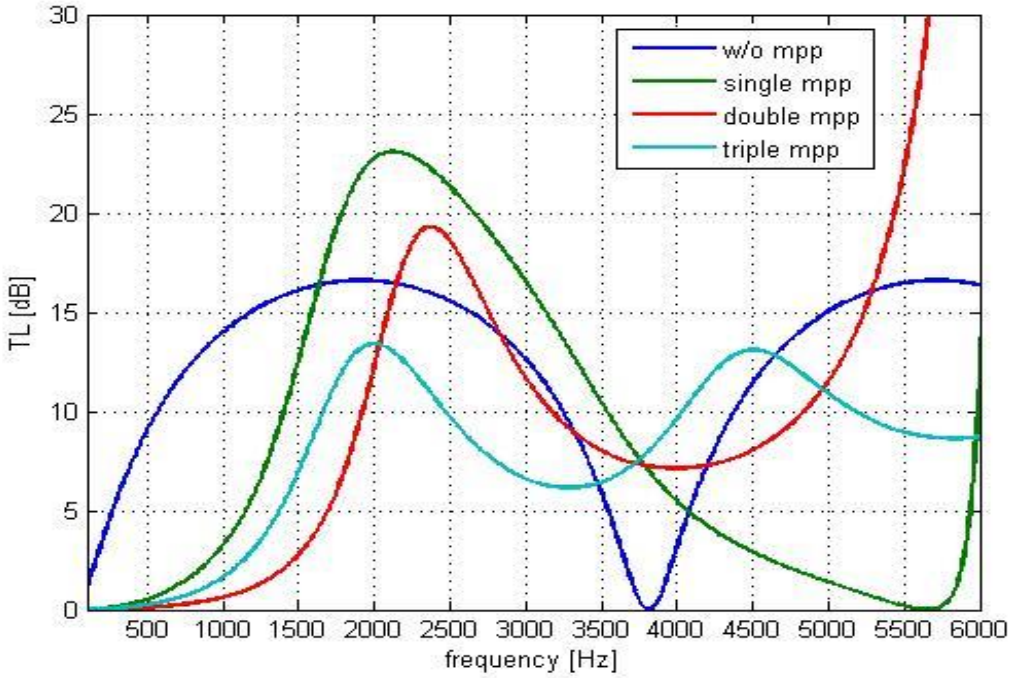

Figure 9.7. Comparison of transmission loss of muffler with or without microperforated liners.

The genetic algorithm was used to perform the optimization, and the parameters that were varied were thickness, hole diameter, porosity, and mass per unit area of each panel, and the distance between the panels if there was more than 1 panel. The error function was $1/TL$ averaged over the frequency range 500 to 4000 Hz: i.e., the speech interference range. The limits on the panel parameters were: diameter of hole, 0.0001 to 0.0003 m; thickness of panel, 0.0002 to 0.0008 m; porosity, 0.01 to 0.2; and mass per unit area, 0.3 to 0.6 kg/m^2. The optimization was performed for one to five microperforated panels. These constraints are shown in Table 9.1.

Table 9.1. Constraints of components.

	Minimum	Maximum
N	1	5
t [mm]	0.2	0.8
d [mm]	0.1	0.3
σ	0.01	0.2
m [kg/m^2]	0.1	0.8
l [m]	0.001	0.2
M [kg/m^2]		3
L [m]		0.32

And also, to make comparison with optimization result, the maximum resistance set and the minimum resistance set were used and the parameters of the two set are given in Tables 9.2 and 9.3.

Table 9.2. Maximum resistance set.

t [mm]	0.8
d [mm]	0.1
σ	0.01
m [kg/m^2]	3/N
l [m]	0.5/N
M [kg/m^2]	3
L [m]	0.32

Table 9.3. Minimum resistance set.

t [mm]	0.2
d [mm]	0.3
σ	0.2
m [kg/m^2]	0.3
l [m]	0.5/N
M [kg/m^2]	3
L [m]	0.32

Figure 9.8 shows the optimization result for the one to five microperforated panel cases in the cylindrical duct, and Table 9.4 lists the properties of the optimal model for the five layer MPP liner which can be seen to give the best performance. Recall that the transmission losses are given here in decibels per 0.045 m, and for reference are compared to the transmission loss of a simple expansion muffler, also of 0.045 m in length (and with an inlet radius, 0.012 m, and an expanded section radius, 0.044 m).

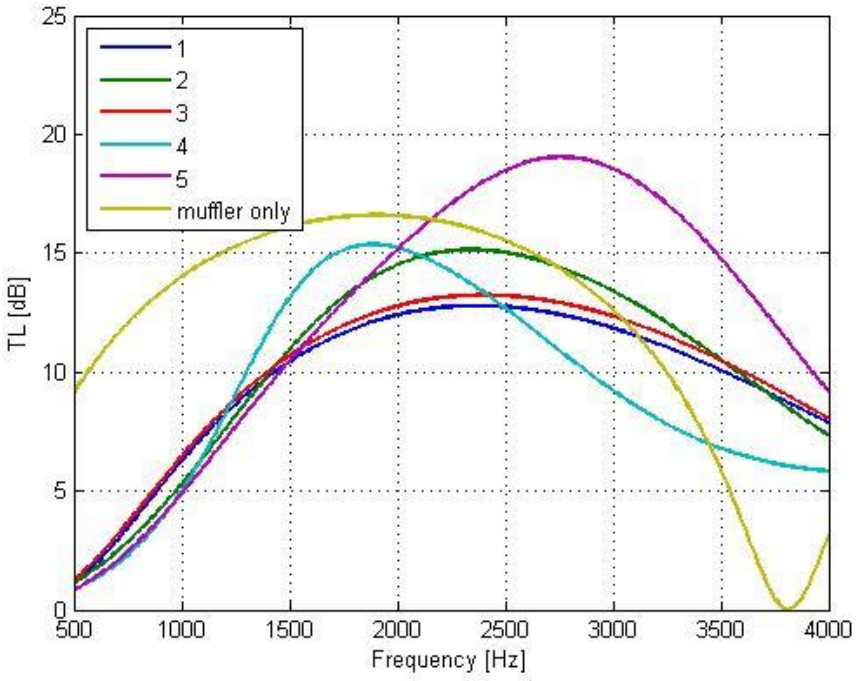

Figure 9.8. Comparison of transmission loss of lined duct section 0.045 m in length and a simple expansion muffler of the same length.

Table 9.4. Optimal model properties of 5 layers of MPP liner.

	Thickness [mm]	Diameter [mm]	Porosity	Mass per unit area [kg/m^2]	Distance to next panel [m]
Panel 1	0.2191	**0.1000**	0.1625	0.31028	0.0145
Panel 2	**0.2000**	**0.1000**	0.0101	**0.6**	0.0010
Panel 3	**0.2000**	**0.3000**	0.0842	**0.3**	0.0010
Panel 4	**0.2000**	**0.3000**	0.0110	**0.3**	0.0146
Panel 5	**0.2000**	**0.3000**	0.2000	**0.3**	

Figure 9.9 shows that acoustic performance of optimized multi-layer duct liners is much better than of with maximum resistance set. Transmission loss of maximum resistance set is below 5 dB over the whole frequency range.

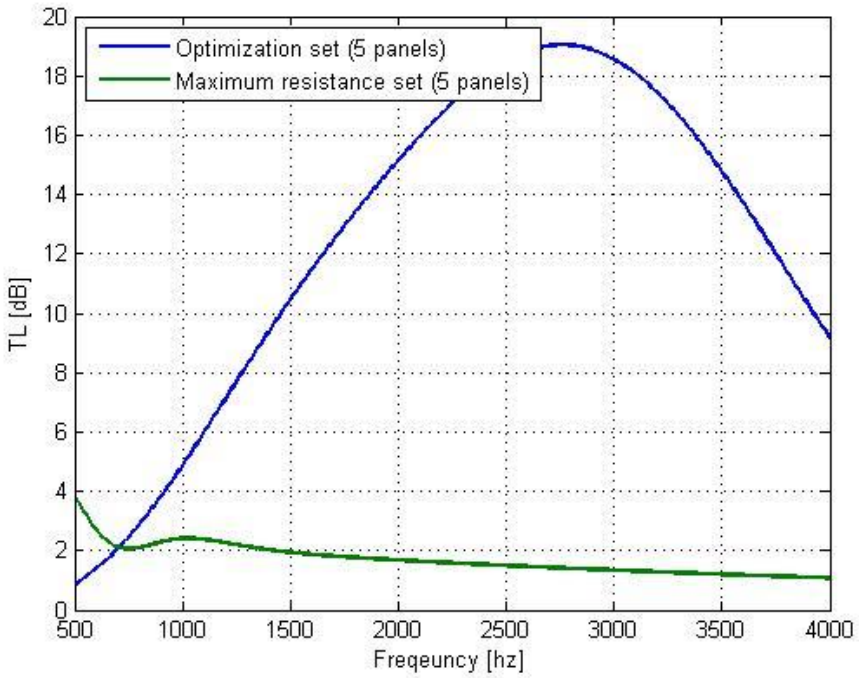

Figure 9.9. Comparison of transmission loss of 5 panels optimized set and maximum resistance set.

As shown in Figure 9.10, the transmission loss of the minimum resistance set provides better performance than that of optimized set in the frequency range over about 2300 Hz. However, recall that one of the goals of the optimization is to remove minima in the transmission loss. From this point-of-view, the minimum resistance set has too low a transmission loss in the range under 1500 Hz, so this set is not fit for our purpose.

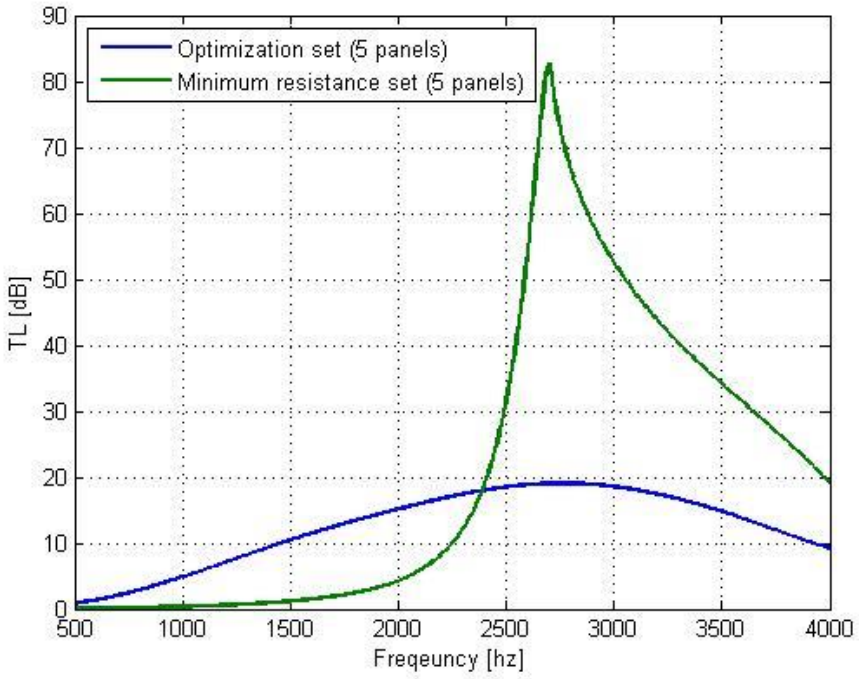

Figure 9.10. Comparison of transmission loss of 5 panels optimized set and minimum resistance set.

9.3 Summary

The objective of the work described in this chapter was to maximize the transmission loss of a lined duct in the 500 to 4000 Hz range. A simple expansion muffler without any lining actually gives better average performance than the lined duct. However, in the muffler case, there is a resonance frequency at about 3800 Hz that is related to the length of the muffler, and which causes the transmission loss to drop to

zero, which is clearly undesirable. In contrast, the duct liner optimization shows the possibility of creating a relatively high transmission loss over a broad range of frequencies with a relatively short lined duct length. And note that while the use of multiple duct liners may reduce the maximum transmission loss in a specific frequency range, at the same time the use of multiple liners makes it possible to shift resonances, and the resulting zeroes in the Transmission Loss spectrum, out of the frequency range of interest. And it is certainly true that an appropriate combination of thickness, hole diameter, porosity, and mass per unit area of microperforated panels can yield a good solution for particular conditions.

CHAPTER 10. CONCLUSIONS AND FUTURE WORK

10.1 Conclusions

In this study, optimal designs for three different types of sound absorbing system have been considered: a single panel system, a multi-layer system, and a duct liner. The optimization results show some possibilities to make the sound absorbing system lighter or smaller.

For the single microperforated panel with tapered holes, the proper combination of MPP properties can give desirable performance. Especially, the relation between porosity and angle of the hole shows the possibility to create the same performance with fewer holes. However it showed also the limitation on covering a wide range of frequency.

For multi-layer microperforated system, barrier and a functional absorber cases were considered. The result shows that the proper combination of multi-layer panels can cover a wide range of frequencies: here, the speech interference range. For a barrier case, this optimal design can remove the internal resonance frequencies, and for the functional absorber, the performance can be much improved compared to just using the panels with the maximum resistance.

For the duct liner, the optimization result shows the possibility to make mufflers shorter with the same performance by shifting the resonance frequency. The muffler

without any liner has the best performance if you can make it long enough, but there are lots of limitations in the real world. So by using microperforated panels as duct liners that can be one of the answers to cover a specific range of frequencies.

10.2 Future Work

In this thesis, only the locally reacting case was considered. If the optimization can be performed for the extended reaction case, then the design of multi-layers of microperforated panel systems, especially without internal segmentation, can be achieved by optimization. Also, here, the edge constraint was not considered. If optimization process can also calculate the effect of edge constraint on the performance of flexible microperforated panels, then the size of multi-layers systems can also be decided. These two subject can help in the design of multi-layers systems to be used in the industrial field.

LIST OF REFERENCES

LIST OF REFERENCES

Bolt, R. H. (1947). On the design of perforated facings for acoustic materials, *Journal of the Acoustical Society of America*, 19(5): 917-921.

Bolton, J. S., & Kim, N.N. (2010). Use of CFD to calculate the dynamic resistive end correction for microperforated materials, *Acoustics Australia*, 38(3): 129-134.

Booker, L. (1987). Improving search in genetic algorithms. Genetic Algorithms and Simulated Annealing: 61-73 Morgan Kaufmann Publishers.

Caruana, R. A., Eshelman, L. A., & Schaffer, J. D. (1989). Representing and hidden bias II: Eliminating defining length bias in genetic search via shuffle crossover. *Proceedings of the Eleventh International Joint Conference on Artificial Intelligence*: 750-755 Los Altos, Cal.:William Kaufmann, Inc.

Chipperfield, A., & Fleming, P. J. (1996). Multiobjective gas turbine engine controller design using genetic algorithms. *IEEE Transactions on Industrial Electronics* 43(5): 583-587.

Chipperfield, A. J., Bica, B., & Fleming, P. J. (2002). Fuzzy Scheduling Control of a Gas Turbine Aero-Engine: A Multiobjective Approach. *IEEE Transactions on Industrial Electronics* 49(3): 536-548.

Chipperfield, A. J., Fleming, P. J., & Pohlheim, H. P. (1994). A Genetic Algorithm Toolbox for MATLAB. *Proceedings of the International Conference Systems Engineering*, Coventry, UK: 200-207.

Crandall, I.B. (1926). Theory of Vibrating Systems and Sound, New York: Van Nostrand, pp. 229.

Deb, K. (2001). Multi-Objective Optimization using Evolutionary Algorithms, John Wiley & Sons, Chichester, UK.

Deb, K., & Agrawal, R. B. (1995). Simulated Binary Crossover for Continuous Search Space. *Complex Systems* 9: 115--148.

Deb, K., & Goyal, M. (1996). A combined Genetic Adaptive Search (GeneAS) for Engineeriong Design. *Computer Science and Informatics* 25(4): 30-45.

Fonseca, C. M. (1994). Multiobjective Genetic Algorithms with Applications to Control Engineering Problems. PhD Thesis, Department of Automatic Control and Systems Engineering. Sheffield, UK, University of Sheffield.

Fonseca, C. M., & Fleming, P. J. (1993). Genetic algorithms for multiobjective optimisation: Formulation, discussion and generalization. *Proceedings of the fifth international conference on genetic algorithms*, San Mateo, USA: 416–423.

Fonseca, C. M., & Fleming, P. J. (1994). Multiobjective optimal controller design with genetic algorithms. *Proceedings of the IEE Control Int. Conf*, UK: 745-749.

Fonseca, C. M., & Fleming, P. J. (1995). Multiobjective Genetic Algorithms Made Easy: Selection, Sharing and Mating Restriction. Evolutionary Computation. *Proc. 1st IEE/IEEE International Conference on Genetic Algorithms in Engineering Systems: Innovations and Applications*, Galesia: 45-52. 154.

Fonseca, C. M., & Fleming, P. J. (1998a). Multiobjective optimization and multiple constraint handling with evolutionary algorithms. I. A unified formulation. *IEEE Transactions on Systems, Man and Cybernetics-Part A: systems and humans* 28(1): 26-37.

Fonseca, C. M., & Fleming, P. J. (1998b). Multiobjective optimization and multiple constraint handling with evolutionary algorithms. II. Application example. *IEEE Transactions on Systems, Man and Cybernetics-Part A: systems and humans* 28(1): 38-47.

Goldberg, D. E. (1989). Genetic Algorithms in search, optimization and machine learning. Reading, MA, Addison Wesley.

Guo, Y., Allam, S., & Abom, M. (2008). Micro-perforated plates for vehicle applications. *INTER-NOISE 2008*, Shanghai, China.

Herdtle, T., Bolton, J. S., Kim, N. N., Alexander, J. H., & Gerdes, R. W. (2013). Transfer impedance of microperforated materials with tapered holes, *Journal of the Acoustical Society of Am*erica, 134(6), Pt. 2

Holland, J. H. (1975). Adaptation in natural and artificial systems. Ann Arbor, The University of Michigan Press.

Hou, K., & Bolton, J. S. (2009). Finite element models for micro-perforated panels. *INTER-NOISE 2009*, Ottawa, Canada.

Ingard, U. (1953). On the theory and design of acoustic resonators, *Journal of the Acoustical Society of America*, 25: 1037-1061.

Ingard, U., & Bolt, R. H. (1951). Absorption characteristics of acoustics material with perforated facings, *Journal of the Acoustical Society of America*, 23(5): 553-540.

Ingard, U., & Lyon, R. H. (1953). The impedance of a resistance loaded Helmholtz resonator, *Journal of Acoustical Society of America*, 25(5): 854-857.

Kim, N. N., & Bolton, J. S. (2011). Use of CFD to calculate the transfer impedance of microperforated materials having round-edged holes, *NOISE-CON 2011*, Portland, Oregon, USA.

Kim, N. N., & Bolton, J. S. (2012). CFD Modeling of Tapered Hole Microperfoated Panels, *Proceeding of Inter-Noise 2012*, New York City, USA,.

Kim, N. N., & Bolton, J. S. (2014). Optimization of multi-layer microperforated systems for absorption and transmission loss, *Proceeding of NOISE-CON 2014*, Fort Lauderdale, Florida, USA.

Lai, H., Katragadda, S., Bolton, J. S., & Alexander J. H. (1997). Layered Fibrous Treatments for a Sound Absorption and Sound Transmission, *SAE Technical Paper 972064*, doi:10.4271/972064.

Maa, D. Y. (1975). Theory and design of microperforated panel sound-absorbing constructions, *Scientia Sinca*, 18(1): 55-71.

Maa, D. Y. (1987). Microperforated-panel wideband, *Noise Control Engineering Journal*, 29(3): 77-84.

Maa, D. Y. (1998). Potential of microperforated panel absorber, *Journal of Acoustical Society of America*, 104(5): 2861-2866.

Maa, D. Y. (1999). Statistical absorption coefficient of microperforated absorbers, *Chinese Journal of Acoustics*, 19(2): 97-104.

Melling, T. H. (1973). The acoustic impedance of perforates at medium and high sound pressure levels, *Journal of Sound and Vibration*, 29(1): 1-65.

Morse, P. M., & Ingard, U. (1968), *Theoretical Acoustics*, Princeton: Princeton University Press.

Panton, R. L., & Miller, J. M. (1975). Resonant frequencies of cylindrical Helmholtz resonators. *Journal of the Acoustical Society of America*, 57(6 II): 1533-1535.

Pierce, A.D. (1989). *Acoustics: An Introduction to its Physical Principles and Application*, New York: Acoustical Society of America, pp. 107-200.

Randeberg, R. T. (2000). Perforated panel absorbers with viscous energy dissipation enhanced by orifice design, Ph.D. thesis, Norwegian University of Science and Technology.

Rayleigh, J. W. S. (1894). *Theory of Sound*, New York: Van Nostrand. pp. 323 and 487.

Sakgami, K., Morimoto, M., Yairi, M., & Minemura, A. (2008). A pilot study on improving the absorptivity of a thick microperforated panel absorber, *Applied Acoustics*, 69(2): 179-182.

Song, B. H., & Bolton, J. S. (2000). A transfer-matrix approach for estimating the characteristic impedance and wave numbers of limp and rigid porous material, *Journal of the Acoustical Society of America*, 107(3): 1131-1152.

Stinson, M. R., & Shaw, E.A.G. (1985). Acoustic impedance of small, circular orifices in thin plate. *Journal of the Acoustical Society of America*, 77(6): 2039-2042.

Yoo T. (2008). The modeling of sound absorption by flexible micro-perforated panel, Ph. D. thesis, Purdue University.

Yoo, T., & Bolton, J. S. (2007). An improved model for microperforated absorbers, *NOISE-CON 2007*, Reno, Nevada, USA.

Versteeg, H.K., & Malalasekera, W. (1999). An Introduction to Computational Fluid Dynamics. England: Longman Scientific & Technical.

VITA

VITA

Nicholas Kim was born in Los Angeles, California. He received his B.S. degree in Mechanical Engineering from Seoul National University in Seoul, Republic of Korea in 2009, and he received his master's degree in Mechanical Engineering from Purdue University in 2011. He started Ph.D. program in Mechanical Engineering from Purdue University in 2012 and worked as a Research Assistant for Professor J. Stuart Bolton from 2012 to 2016. He received his Ph.D. degree from Purdue University in December 2016.